Chemical Science

ROYAL SOCIETY OF CHEMISTRY

PERSPECTIVE

View Article Online
View Journal | View Issue

Cite this: *Chem. Sci.*, 2024, **15**, 17739

All publication charges for this article have been paid for by the Royal Society of Chemistry

A perspective on next-generation hyperfluorescent organic light-emitting diodes

Upasana Deori, [a] Gyana Prakash Nanda, [a] Caroline Murawski [bc] and Pachaiyappan Rajamalli *[a]

Hyperfluorescence, also known as thermally activated delayed fluorescence (TADF) sensitized fluorescence, is known as a next-generation efficient and innovative process for high-performance organic light-emitting diodes (OLEDs). High external quantum efficiency (EQE) and good color purity are crucial parameters for display applications. Hyperfluorescent OLEDs (HF-OLEDs) take the lead in this respect as they utilize the advantages of both TADF emitters and fluorescent dopants, realizing high EQE with color saturation and long-term stability. Hyperfluorescence is mediated through Förster resonance energy transfer (FRET) from a TADF sensitizer to the final fluorescent emitter. However, competing loss mechanisms such as Dexter energy transfer (DET) of triplet excitons and direct charge trapping on the final emitter need to be mitigated in order to achieve fluorescence emission with high efficiency. Despite tremendous progress, appropriate guidelines and fine optimization are still required to address these loss channels and to improve the device operational lifetime. This perspective aims to provide an overview of the evolution of HF-OLEDs by reviewing both molecular and device design pathways for highly efficient narrowband devices covering all colors of the visible spectrum. Existing challenges and potential solutions, such as molecules with peripheral inert substitution, multi-resonant (MR) TADF emitters as final dopants, and exciplex-sensitized HF-OLEDs, are discussed. Furthermore, the operational device lifetime is reviewed in detail before concluding with suggestions for future device development.

Received 15th August 2024
Accepted 7th October 2024

DOI: 10.1039/d4sc05489j

rsc.li/chemical-science

1. Introduction

The study of organic light-emitting diodes (OLEDs) is considered one of the research fields that equally drive both academia and industry at the same time. Since the fabrication of the first OLED device by Tang and VanSlyke,[1] this forefront technology has come a long way and has evolved continuously to date. Especially in the display market, the field has rapidly expanded over the years as OLEDs can be integrated to enable self-emissive displays with very high pixel density (500 ppi and beyond) that provide true dark tones. Furthermore, OLEDs can be made transparent and flexible, which enables applications such as wearables, signage, or packaging that require form factors beyond rigid, opaque devices.[2–4]

In an OLED, the electrically generated holes and electrons recombine in the emissive layer and produce 25% excitons in the singlet state and the remaining 75% in the triplet state, according to spin statistics.[5] Initial research started with fluorescent emitters due to their simple structures, which can exhibit unity photon conversion efficiency in the photoluminescence process upon optical excitation.[1,6,7] However, upon electrical excitation, fluorescent emitters can utilize only singlet excitons to emit light, while triplet excitons are lost by non-radiative processes, resulting in a maximum internal quantum efficiency (IQE) of 25%.[8–11] The external quantum efficiency (EQE) of an OLED can be calculated from the expression:[12–15]

$$\mathrm{EQE} = \varphi_{\mathrm{PL}} \times \eta_{\mathrm{r}} \times \gamma \times \eta_{\mathrm{op}}$$

where φ_{PL} is the effective radiative efficiency of the emitter, η_{r} is the so-called spin factor (the theoretical limit of emissive excitons; 25% for a fluorescent OLED), γ is the recombination efficiency, ideally 100%, and η_{op} is the optical outcoupling efficiency, which can reach approximately 20% if layer thicknesses are optimized such that the emitter dipoles are situated at the optical maximum of the electromagnetic field, assuming isotropic emitter orientation. Even if the effective radiative efficiency (based on a very high photoluminescence quantum yield (PLQY)) is considered to be unity, the maximum EQE for fluorescent OLEDs is limited to only 5%. Complete utilization of the generated excitons is crucial to obtain high-efficiency OLEDs. To improve the EQE from 5%, heavy metal complexes such as iridium and platinum-based phosphorescent emitters

[a]*Materials Research Centre, Indian Institute of Science, Bangalore 560012, Karnataka, India. E-mail: rajamalli@iisc.ac.in*

[b]*Kurt-Schwabe-Institut für Mess- und Sensortechnik Meinsberg e.V., Kurt-Schwabe-Straße 4, 04736 Waldheim, Germany*

[c]*Faculty of Chemistry and Food Chemistry, Faculty of Electrical and Computer Engineering, Technische Universität Dresden, 01062 Dresden, Germany*

were developed.[16–18] The noble metal atoms can promote efficient spin–orbit coupling (SOC) by mixing singlet and triplet states, thus enabling the triplet excitons to emit and harvest all generated excitons.[17,19,20] However, the high-EQE phosphorescent emitters are expensive and do not satisfy production costs.[21] Moreover, the stability of blue phosphorescent emitters is a major issue due to their short operational lifetime.[22,23] Over the decades, purely organic thermally activated delayed fluorescence (TADF) emitters have emerged, realizing 100% IQE through reverse intersystem crossing (RISC) ensuing from a small energy gap ($\Delta E_{ST} \lesssim 200$ meV) between the lowest excited singlet (S_1) and triplet (T_1) states.[24–28] The device performance of TADF OLEDs gradually matched with that of phosphorescent OLEDs and even reached an EQE of up to 40%.[29,30] However, TADF emitters have long triplet exciton lifetimes,[31] causing poor device stability and severe efficiency roll-off at high luminance.[32] Also, TADF emitters have a broad spectrum due to their intramolecular charge transfer (ICT) state, resulting in low color purity.[33] Therefore, new approaches are essential to resolve these challenges and to further enhance efficiency, lifetime, and color purity. Fig. 1 shows the timeline and properties of various generations of OLED emitters.

Compared to phosphorescent and TADF emitters, conventional fluorescent emitters usually show narrowband emission with a full width at half maximum (FWHM) value of the OLEDs being less than 70 nm.[34,35] A narrow spectrum is essential for obtaining color saturation, which is a critical requirement for the display industry. Yet, the problem of low-efficiency OLEDs still remains with fluorescent emitters. Recently, there has been a big leap in the device performance in fluorescent OLEDs by harvesting triplet excitons through an energy transfer mechanism from an assistant dopant or a sensitizer. This energy transfer approach is known as hyperfluorescence or TADF-sensitized fluorescence, which is becoming a cornerstone in developing an alternative strategy for next-generation high-performance OLED technology. The hyperfluorescent OLED (HF-OLED) technology combines a highly efficient TADF emitter as a sensitizer and a narrowband fluorescent emitter.[36,37] Due to their spectral behaviour (Fig. 2a), hyperfluorescence could be the solution for OLED displays[38] as it utilizes the advantages of both materials, holding enormous potential to achieve high EQE with narrowband emission and high stability. The primary energy transfer process is Förster energy transfer (FRET) from the lowest excited singlet state of the TADF emitter to the lowest singlet state of the final fluorescent dopant. However, during the process, several energy loss channels, such as Dexter energy transfer (DET) from the triplet state of the TADF emitter to the triplet state of the fluorescent emitter and direct charge trapping on the final fluorescent emitter can also take place and need to be blocked as these can deteriorate the device performance.[39,40] Research towards HF-OLEDs is ongoing to improve their efficiency and lifetime. The confinement of all generated excitons in the multicomponent emissive layer and reduced carrier accumulation at the interfaces are also essential for maximizing the device performance. A simplified device structure of multilayer OLEDs is shown in Fig. 2b.

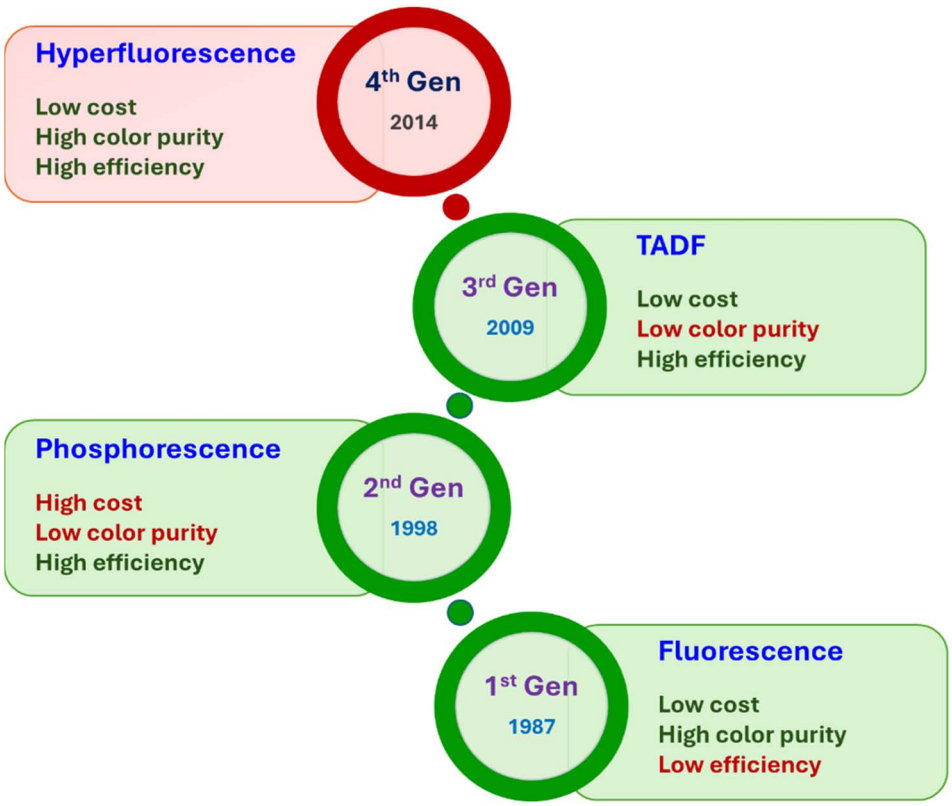

Fig. 1 Timeline and properties of the different generations of OLED emitters.

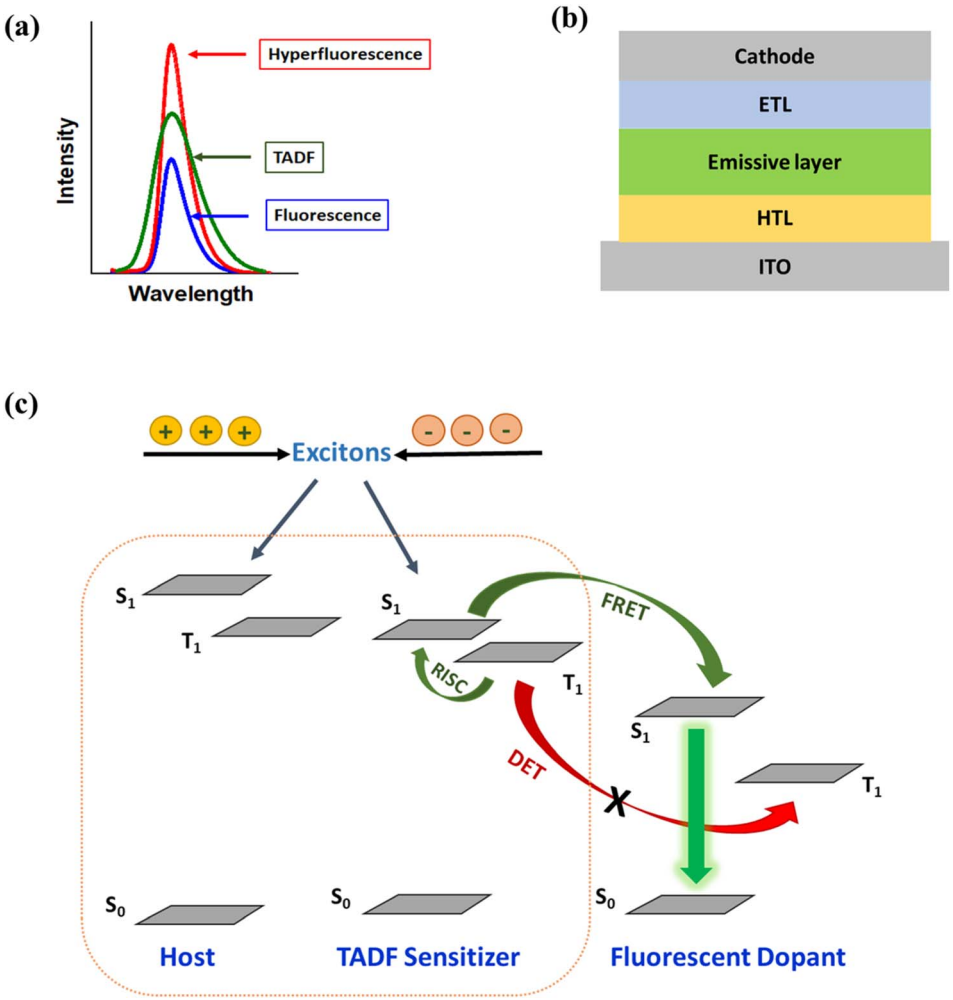

Fig. 2 (a) Spectral behaviour of fluorescent, TADF and hyperfluorescent devices. (b) A simplified device structure of multilayer organic light-emitting diodes: ITO (indium tin oxide)/HTL (hole transporting layer)/emissive layer/ETL (electron transporting layer)/cathode. (c) A schematic diagram of energy transfer processes in a hyperfluorescent device.

In this perspective, the evolution of HF-OLEDs across all emission colors and current challenges are discussed in detail. Several recent approaches have been investigated to improve the overall performance of the multilayer HF-OLEDs. With color purity being a crucial parameter for display applications, various narrowband emitters which can be used as a final dopant are mentioned. HF-OLEDs can harvest triplet excitons, thereby reducing the excited state lifetime of the emissive layer and minimizing degradation. With the help of appropriate molecular designs and device engineering, these devices have the potential to achieve high EQE and extended operational lifetimes. This perspective focuses on material requirements, device structures and the suppression of energy loss mechanisms to achieve high-performance HF-OLEDs. There are many competitive potential materials that have emerged as sensitizers for fluorescent OLEDs, such as organic phosphorescent dyes[41,42] and hybridized local and charge-transfer (HLCT) emitters;[43,44] however, this perspective will focus solely on TADF-based sensitizers and their contribution to HF-OLEDs. Finally, an outlook providing suggestions to further improve the performance of HF-OLEDs is presented.

2. Working principle

The concept of hyperfluorescence combines a host, a highly efficient TADF material, and a narrow-spectrum fluorescent emitter that can achieve 100% IQE. The detailed mechanism of hyperfluorescence is shown in Fig. 2c. Upon electrical excitation, charge carriers are injected, which recombine to form excitons in the singlet and triplet states. The role of the TADF molecule is to enable efficient up-conversion of excitons from the triplet state into the singlet state *via* RISC and then to transfer the singlet state exciton to the final fluorescent guest emitter, where it will decay and emit a photon. In this approach, the TADF material, which is introduced as an assistant dopant or sensitizer, should have a high PLQY and must possess a high RISC rate in order to efficiently up-convert and harvest all excitons that are formed. Eventually, the fluorescent emitter is now capable of achieving three times higher device efficiency than conventional fluorescent devices that do not use sensitizers.[45] The singlet and triplet energy levels of the materials should be appropriately aligned to maximize exciton

confinement in the multicomponent emissive layer, and the triplet energy level of the host should be higher than those of both TADF and fluorescent emitters to prevent energy back transfer.

The main energy transfer process in an HF system is the long-range FRET process. Efficient FRET can be realized by ensuring sufficient spectral overlap between the emission spectrum of the TADF sensitizer and the absorption spectrum of the final fluorescent emitter. For efficient hyperfluorescence, the fraction of excited state energy that is transferred from the TADF sensitizer to the fluorescent emitter should be sufficiently high in order to achieve high FRET efficiency.[46] This also minimizes potential emission from the TADF sensitizer by proper FRET management, hence increasing the color purity of the HF-OLEDs. The doping concentration of the fluorescent emitter in the emissive layer should be optimized in a way that ensures singlet energy transfer while minimizing loss processes like DET of triplet excitons and direct charge trapping.[47] The energy transfer process between the sensitizer and final dopant can be explained with the help of FRET theory.[48] The rate constant of the FRET (k_{FRET}) process can be expressed as:

$$k_{FRET} = \frac{1}{\tau_D}\frac{{R_0}^6}{R^6},$$

where τ_D is the prompt decay lifetime of the TADF sensitizer in the absence of the final dopant, R is the average molecular distance between the TADF sensitizer and fluorescent emitter, and R_0 is the Förster radius. Furthermore, the energy transfer efficiency (Φ_{ET}) from the TADF sensitizer to the fluorescent emitter can be calculated from:

$$\Phi_{ET} = \frac{k_{FRET}}{k_{FRET} + \frac{1}{\tau_D}} = \frac{1}{1 + \frac{R^6}{{R_0}^6}}$$

with

$${R_0}^6 = \frac{9000\ln(10)\kappa^2\varphi_f}{128\pi^5 n^4 N_A}\int_0^\infty F_D(\lambda)\varepsilon_A(\lambda)\lambda^4 d\lambda$$

Here, κ^2 is the relative dipole orientation factor, taken as 2/3 assuming isotropic orientation,[49] n is the refractive index, assumed to be 1.8 for most organic materials,50 N_A is Avogadro's constant, φ_f is the PLQY of the TADF sensitizer, and $\int_0^\infty F_D(\lambda)\varepsilon_A(\lambda)\lambda^4 d\lambda$ is the spectral overlap integral between the PL emission of the sensitizer with the absorption of the final dopant.[51] Thus, for high Φ_{ET}, the spectral overlap integral and PLQY of the sensitizer need to be maximized. A highly efficient TADF sensitizer with an efficient FRET would suppress the loss processes and enable the development of high-performance OLEDs.

3. Evolution of hyperfluorescent OLEDs

Adachi and co-workers demonstrated the first HF-OLED in 2014, in which they used TADF molecules as sensitizers or assistant dopants to transfer electrically generated excitons to the final fluorescent emitters.[36] The group reported highly efficient blue, green, red, and yellow HF-OLEDs with EQE_{max} ranging from 13% to 18%. Following that, several groups used this strategy to develop high-efficiency and pure color OLEDs. Kyulux also demonstrated impressive HF-OLEDs with narrow emission, providing high color purity.[38] In order to enhance the OLED performance further, various modifications in the molecular design and in device structures have been investigated. Here, we will discuss the evolution of HF-OLEDs based on fluorescent emitters, covering the primary colors blue, green, and red, as well as white light devices. Some of the molecular structures of TADF sensitizers and fluorescent dopants are

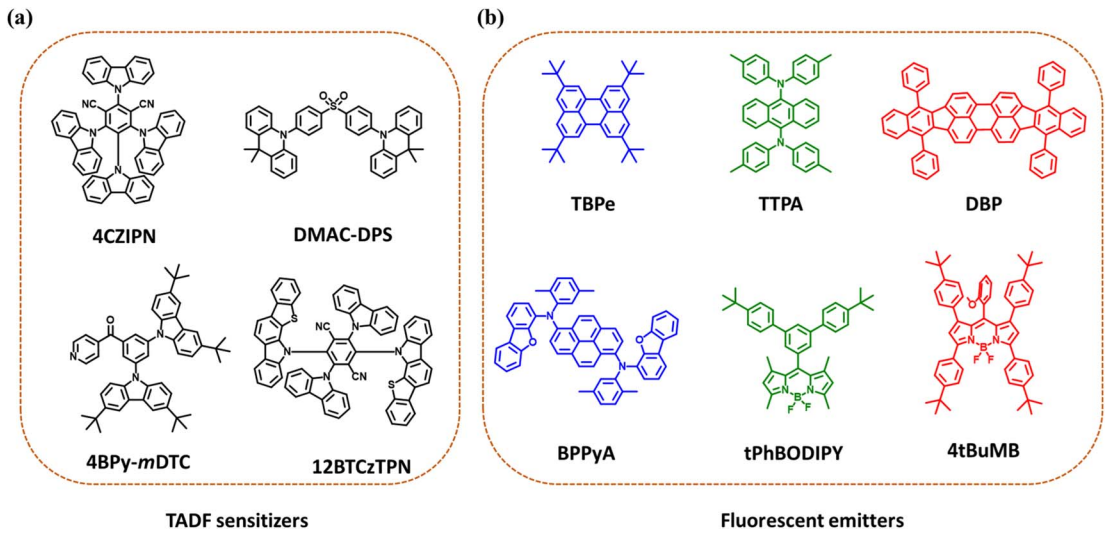

Fig. 3 (a) Molecular structures of TADF emitters used as sensitizers for hyperfluorescent OLEDs. (b) Molecular structures of various blue, green and red fluorescent emitters used as final dopants.

shown in Fig. 3a and b. The performances of HF-OLEDs using fluorescent dopants are summarized in Table 1.

3.1 Blue hyperfluorescent OLEDs

High efficiency and long lifetime remain significant challenges for blue OLEDs as compared to red, yellow, and green OLEDs, because the wider bandgap of blue light leads to faster material degradation and, hence, shortened device operational lifetime. This is particularly true for deep blue phosphorescent and TADF emitters,[23,80,81] where the high emission energy and long triplet exciton lifetime[82] contribute to the generation of highly reactive 'hot excited states' through exciton annihilation processes.[83] These are also lethal to the surrounding organic materials, thus particularly restricting device operational lifetimes. Fluorescent emitters instead possess much lower exciton lifetimes, which strongly improve device stability. For this reason, they are still in use for practical display and lighting applications, even though they provide much lower EQE.

Utilizing the benefits of fluorescent emitters, HF-OLEDs came into existence. The first HF blue OLED demonstrated by Nakanotani *et al.* showed an efficiency of 13% using the TADF sensitizer ACRSA with the fluorescent emitter TBPe.[36] With time, various new molecular designs for blue TADF molecules have emerged, which can be utilized as sensitizers to deliver improved performance. Song *et al.* reported a blue-emitting TADF compound, CzAcSF, as the triplet-sensitizing host to efficiently transfer emission energy to TBPe without any external host.[52] The CzAcSF molecule consisted of a weak diphenyl sulfone acceptor with moderate acridine and carbazole donors, which increased the band gap of CzAcSF towards deep blue emission. The EQE_{max} for the HF system was 15.4%, showing an enhancement from the ACRSA:TBPe system discussed above.[36] The efficiency of the blue HF-OLED increased to 18.1% by incorporating the wide band gap DPEPO host in the emissive layer.[84] Kang *et al.* designed two TADF sensitizers, *t*DCztTrz and *t*DCz2*t*Tz, based on a triazine derivative with peripheral alkyl branches around the core, which led to an EQE

Table 1 Hyperfluorescent OLEDs based on fluorescent dopants

Final dopant	Sensitizer	Host	EL (nm)	FWHM (nm)	EQE_{max}/ 1000 cd m^{-2} (%)	PE_{max}/ 1000 cd m^{-2} (lm W^{-1})	CIE	Ref.
TBPe	ACRSA	DPEPO	—	—	13.4/8.7	18/7	(0.17, 0.30)	36
TTPA	ACRXTN	*m*CP	—	—	15.8/11.7	47/30	(0.29, 0.59)	36
TBRb	PXZ-TRZ	*m*CBP	—	—	18.0/17.2	58/33	(0.45, 0.53)	36
DBP	Tri-PXZ-TRZ	CBP	—	—	17.5/10.9	28/10	(0.61, 0.39)	36
TBPe	CzAcSF	—	—	—	15.4/10.7	23.4/9.7	(0.15, 0.23)	52
TBPe	CzAcSF	DPEPO	—	—	18.1	31.2	(0.15, 0.22)	52
TBPe	*t*DCztTrz	DPEPO	—	—	13.7	—	—	53
TBPe	TpAT-tFFO	CzSi	462	—	18.7/17.1	—	(0.15, 0.23)	54
TBPe	5Cz-TRZ	*m*CBP	—	—	24.0	—	—	55
TBRb	5Cz-TRZ	*m*CBP	—	—	24.9	—	—	55
BPPyA	DMAC-DMT	DBFPO	458	—	19.0	—	(0.14, 0.15)	56
DNTBPe	4TCzBN	DOBNA-OAr	468	63	32.7/18.8	47.7/17.7	(0.14, 0.21)	57
TBPe	4TCzBN	DOBNA-OAr	463	63	24.0/12.6	35.0/12.7	(0.15, 0.23)	57
TBPe	4TCzBN	DCz-BTP	466	—	20.5/16.9	34.7/19.6	—	58
6tBPA	FTrzTCz	DPEPO	517	—	17.9/14.0	—	(0.24, 0.58)	59
6tBPA	TbCzTrz	DPEPO	—	—	14.6/9.2	—	(0.25, 0.57)	60
6tBPA	BPAc	DPEPO	—	—	16.6/15.2	36.0/22.3	(0.23, 0.51)	61
TAA-PPO	4BPy-*m*DTC	*m*CBP	518	—	17.8	48.1	(0.23, 0.58)	62
C545T	PXZ-DPS	DMAC-DPS	—	—	11.1	21.4	—	63
PhtBuPAD	PXZ-DPS	PhCzTrz	—	—	24.0/23.8	71.4/52.3	(0.36, 0.58)	64
C545T	3BPy-*m*DTC	*m*CBP	508	—	23.0	69.9	(0.20, 0.56)	65
*t*PhBODIPY	4CzIPN	DCZDCN	—	32	19.0/18.9	85.7/78.3	(0.26, 0.67)	66
*t*PhBODIPY	4CzIPN	*m*CBP	—	32	18.8/18.6	74.5/53.3	(0.28, 0.67)	67
DBP	TXO-TPA	*m*CBP	—	—	16.9/2.6	27.8/1.8	(0.65, 0.35)	68
DBP	2,7-TXO-PhCz	CBP	—	—	15.9/4.9	31.2/5.5	(0.52, 0.45)	69
4tBuMB	4CzTPN	DIC-TRZ	617	44	19.4/17.2	—	(0.64, 0.36)	70
4tBuMB	12BTCzTPN	DIC-TRZ	618	46	19.9/16.7	—	(0.64/0.36)	71
DBP	FPXZ-DBPZ	CBP	—	—	18.1/—	26/-	(0.61, 0.38)	72
DBP	2BT12CzINN	PBICT:DBTTP1	614	—	14.7	12.7	(0.60, 0.39)	73
TBRb	4CzIPN-Me	*m*CBP	—	—	19.1/16.7	—	(0.43, 0.54)	74
TBRb	PyCNTruX	PBICT	—	—	20.2	50.7/46.5	(0.45, 0.53)	75
Solution-processed HF-OLED								
TBPe	5CzCN	DPOBBPE	—	—	18.8	14.3	(0.14, 0.20)	76
DBP	DC-TC	CBP	—	—	8.0	—	(0.61, 0.38)	77
5TBUPH-BODIPY	phCz-4CzTPN	—	616	47	4.9	—	(0.64, 0.36)	78
Cibalackrot	4CzIPN-*t*Bu	CBP	—	—	15.3/8.4	—	—	79

of 13.7% with the TBPe emitter.[53] The fast RISC rate for the TADF sensitizer is an essential factor for developing efficient HF-OLEDs. Hence, Wada *et al.* designed a TADF emitter, TpAT-tFFO, with a tilted alignment of the donor and acceptor, which exhibited fast RISC (10^7 s^{-1}) due to near-degenerate charge transfer and locally excited triplet states.[54] This fast RISC reduces the concentration of triplet excitons and various annihilation events in the emissive layer. The device achieved an EQE_{max} of 18.7% while sensitizing TBPe with a reduced roll-off and retaining the EQE of 11.8%, even at a high luminance of 10 000 cd m^{-2} (Fig. 4a–c). Cui *et al.* reported a sky-blue TADF molecule, 5Cz-TRZ, which formed charge resonance type triplet states leading to a small ΔE_{ST} and a fast RISC rate (10^7 s^{-1}).[55] The EQE_{max} achieved for the HF-OLED with TBPe was 24.0%. New emitters for final dopants have also emerged to contribute to the HF system. The main requirements are (1) a narrow blue emission spectrum with a wavelength range of 440–470 nm, (2) a small Stokes' shift, and (3) a large spectral overlap with TADF emission. Based on these norms, Ahn *et al.* developed high-efficiency deep-blue HF-OLEDs using BPPyA as a blue fluorescent emitter, which showed an emission maxima of 458 nm with high PLQY (98%).[56] Optimized HF-OLEDs were fabricated using the blue TADF emitters DMAC-DPS, DMAC-DMT and SPAC-DMT as sensitizers. The devices exhibited deep-blue emission from BPPyA, and a maximum EQE of 19.0% was achieved using DMAC-DMT as a sensitizer (Fig. 4d–f). Very recently, Wu *et al.* designed a highly efficient fluorescent emitter by doping nitrogen atoms into polycyclic aromatic hydrocarbons of the TBPe emitter, named DNTBPe.[57] The HF devices were fabricated using the DOBNA-OAr host, 4TCzBN as the TADF sensitizer, achieving an EQE_{max} of 32.7% for DNTBPe and 24.0% for TBPe final dopants.

Although there has been great interest in exploring new blue emitters for HF-OLEDs, the development of host materials for blue devices has considerably lagged. Wang *et al.* reported a pyridine-fused bipolar host, DCz-BTP, which showed a low turn-on voltage of 2.8 V and a maximum EQE of 20.5% using the 4TCzBN sensitizer and TBPe emitter as shown in Fig. 4g–i.[58] The pseudo-symmetric structure of the DCz-BTP host enabled lower driving voltage and enhanced electroluminescence performance as compared to the commonly used traditional hosts such as DPEPO and *m*CBP. Moreover, for solution-processed blue HF-OLEDs, these traditional hosts performed poorly due to their poor solubility. Jeon *et al.* developed a new soluble, high-triplet energy host, DPOBBPE, and demonstrated the first solution-processed blue HF-OLED with the blue TADF compound 5CzCN and TBPe to achieve an efficiency above 18%.[76]

3.2 Green hyperfluorescent OLEDs

Yun *et al.* demonstrated a green HF-OLED with a 6tBPA fluorescent emitter and a triazine derivative sensitizer, FTrzTCz

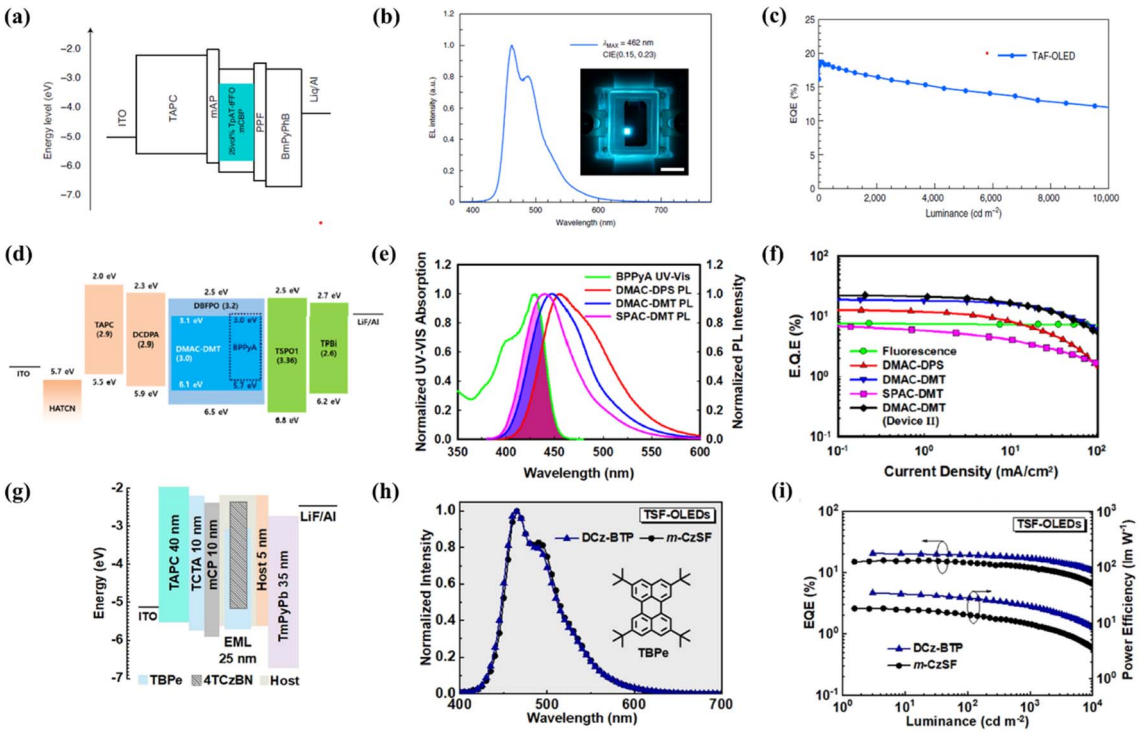

Fig. 4 Blue hyperfluorescent OLEDs. (a–c) Device structure, electroluminescence spectra and efficiency of the *m*CP:TpAT-tFFO:TBPe emissive system. Reproduced with permission from ref. 54, *Nature*, 2020. (d–f) Device structure using DPEPO:DMAC-DMT:BPPyA as an emissive layer, overlap of absorption of BPPyA with the emission spectra of the TADF sensitizers and EQE of all the devices. Reproduced with permission from ref. 56, American Chemical society, 2018. (g–i) Device structure of the hyperfluorescent device with the 4TCzBN sensitizer and TBPe emitter, electroluminescence spectra and EQE–luminance–power efficiency plots. Reproduced with permission from ref. 58, John Wiley and Sons, 2022.

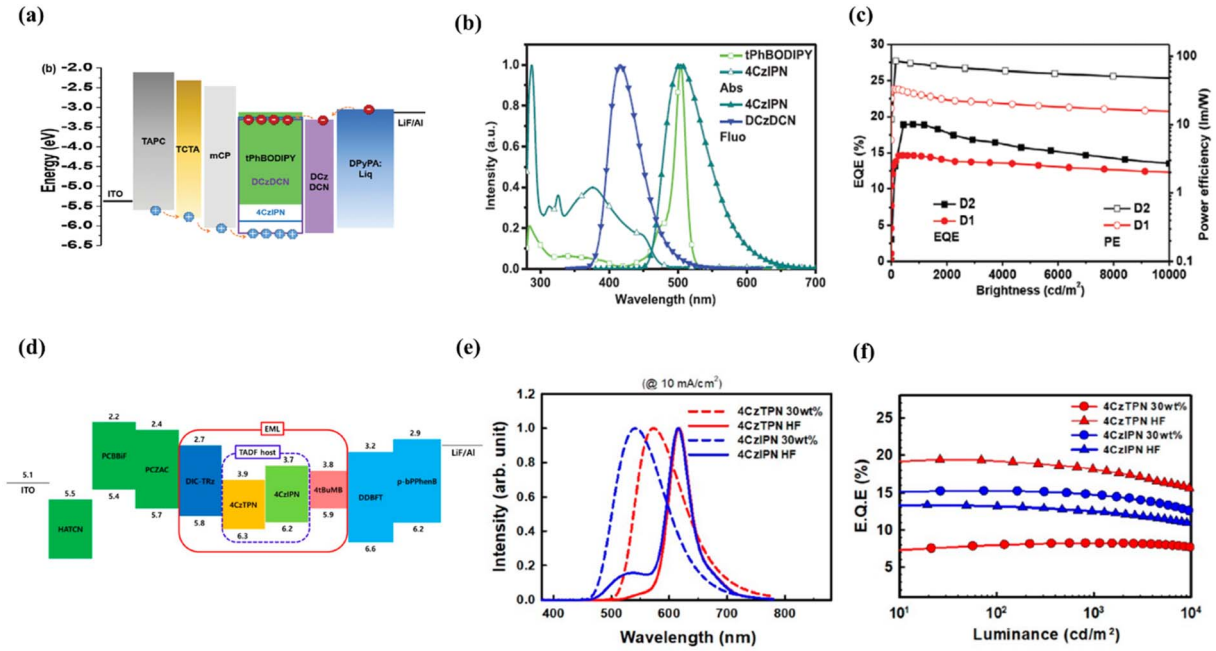

Fig. 5 (a–c) Green hyperfluorescent OLEDs. The device structure used in fabrication, absorption and emission spectra of *t*PhBODIPY and 4CzIPN and the efficiency plot of the devices. Reproduced with permission from ref. 66, John Wiley and Sons, 2020. (d–f) Red hyperfluorescent OLEDs. The device structure of the HF-OLED, electroluminescence spectra of TADF-based and HF-based OLEDs and EQE *vs.* luminance of the devices. Reproduced with permission from ref. 70, American Chemical Society, 2021.

showing an EQE of 17.9%. Incorporating fluorine in the acceptor core of the TADF sensitizer has induced strong charge transfer properties and a fast RISC process.[59] 6tBPA has also been doped with sky-blue TADF sensitizers, TbCzTrz and BPAc, resulting in reasonable performances with EQEs of 14.6% and 16.6%, respectively.[60,61] One of our studies reported an anthracene-based green emitter, TAA-PPO, with an EQE of 7.2% without any sensitizer, and later the device performance was improved up to 17.8% using 4BPy-*m*DTC as the TADF sensitizer.[62] Li *et al.* reported an enhancement of EQE from 9.0% to 11.1% by introducing a synergetic effect using dual-TADF hosts.[63] The introduction of the second TADF emitter established an additional sensitizing route, thereby increasing the FRET rate and reducing exciton loss processes in the HF system. Zhang *et al.* reported a series of green dyes involving N^9,N^9,N^{10},N^{10}-tetraphenylanthracene-9,10-diamine (PAD) as the emissive core.[64] All the emitters (PAD, MePAD, *t*BuPAD, and PhtBuPAD) showed high PLQY (80–89% in toluene solution) and performed well when doped into the TADF sensitizer, PXZ-DPS, for green HF-OLEDs. The HF device achieved an EQE of 24% for the PhtBuPAD-based final emitter. In a recent report, we discussed the importance of appropriate material combinations for green HF-OLEDs by systematic investigation. Optimized energy gaps between the TADF sensitizers and final fluorescent emitters are crucial to improve the performance and reduce EQE roll-off of the devices.[65] Recently, a family of well-known fluorescent emitters, tetracoordinate boron-dipyrromethene (BODIPY) derivatives, have emerged as suitable candidates for use as the final emitter in HF systems.[85,86] BODIPY materials demonstrated high molar extinction coefficients, high PLQY (>90%), and narrowband emission (25–35 nm).[87,88] Using these benefits, Song *et al.* developed an ultrapure green HF-OLED using a BODIPY derivative, named *t*PhBODIPY, as the final dopant, achieving an EQE of 18.9% at a practical luminance of 1000 cd m^{-2} with a narrow FWHM of 32 nm using the TADF sensitizer 4CzIPN (Fig. 5a–c).[66] Nakamura *et al.* also reported highly efficient (EQE: 19%) and stable pure green HF-OLEDs with *t*PhBODIPY and 4CzIPN by using triple hole transporting layers (HTLs) in the device structure to reduce carrier accumulation at the layer interface.[67]

3.3 Red hyperfluorescent OLEDs

There are limited reports on high-performance metal-free red emitters. The main challenge with red materials is their rather low PLQY due to the energy gap law.[89–91] Hence, the design and synthesis of efficient red TADF emitters for conventional TADF-OLEDs face substantial challenges. For a red TADF device, a high singlet radiative rate constant (k_r^S) is required, which can be achieved using planar structures, *i.e.* overlap of the frontier molecular orbitals (FMO), which could lead to a large ΔE_{ST} and, thus, the simultaneous realization of a large k_r^S and small ΔE_{ST} is challenging.[39,92–94] Hence, the TADF materials with a small ΔE_{ST} are used as sensitizers for traditional red fluorescent emitters that possess a large k_r^S to achieve efficient red HF-OLEDs. Adachi *et al.* reported the first red HF system using the TADF molecule tri-PXZ-TRZ as a sensitizer with the well-known fluorescent red emitter DBP and achieved a maximum EQE of 17.5%.[36] The DBP emitter has been widely used in the HF system, and OLEDs have been reported with an EQE of 16.9% with the TADF sensitizer TXO-TPA and 15.9% with the

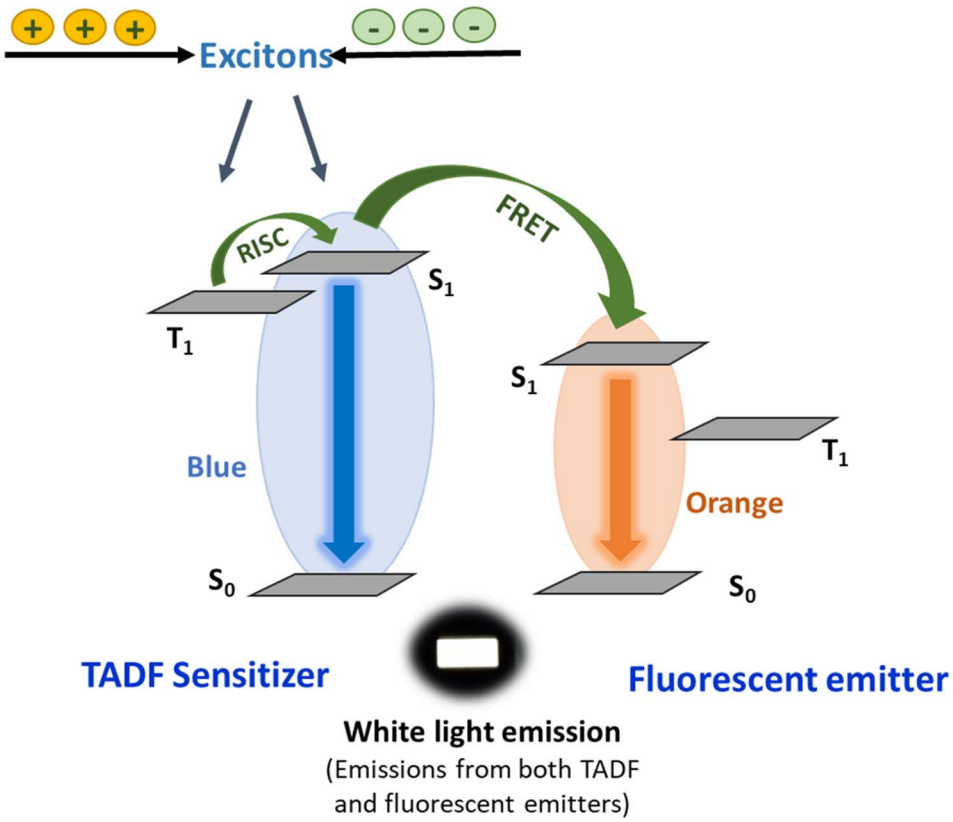

Fig. 6 A schematic representation of white light emission from both the TADF sensitizer and fluorescent emitter.

sensitizer 2,7-TXO-PhCz.[68,69] In both cases, more than 90% energy transfer efficiency was reported from S_1 of the TADF sensitizer to that of DBP, which benefitted in accelerating the RISC process. Red BODIPY materials have also been explored as the final dopant in HF devices. Jung *et al.* fabricated HF-OLEDs using the red BODIPY dopant, 4tBuMB with the TADF sensitizer 4CzTPN and achieved an EQE of 19.4% with a FWHM of 44 nm (Fig. 5d–f).[70] When the assistant dopant was modified to 12BTCzTPN, the device efficiency was slightly enhanced to 19.9% with the same final dopant, 4tBuMB.[71] Several solution-processed red HF devices have been fabricated with both DBP and BODIPY dopants. Using DC-TC as a sensitizer for DBP, the HF device showed an EQE of 8.0%, while the 5TBUPH-BODIPY emitter with the phCz-4CzTPN sensitizer could achieve a maximum EQE of 4.9%.[77,78] Another fluorescent dopant based on the red organic soluble dye cibalackrot was utilized as the final emitter for the solution-processable HF device. The flat and rigid structure of the dye exhibited a high PLQY (96%) and a narrow spectrum (FWHM 37 nm), making it an ideal candidate for electroluminescent devices.[95] Wallwork *et al.* reported an EQE of 15.3% for the solution-processed red HF OLEDs using the cibalackrot dye.[79] Further development of highly efficient organic-based red devices is still in progress, and it would be interesting to see if these metal-free emitter devices could be incorporated into commercial applications.

3.4 White hyperfluorescent OLEDs

Hybrid full-organic white HF-OLEDs based on TADF emitters and fluorescent dopants have gained significant attention for achieving good color quality and high electroluminescence efficiency due to their potential in display panels and general lighting applications.[96–98] One crucial aspect of developing white OLEDs for lighting applications is the color rendering index (CRI), a parameter that indicates how accurately colors of objects are reproduced under particular illumination conditions.[99,100] The CRI should be as high as possible with values above 80 typically being considered suitable for practical lighting applications.[101–103] For achieving such a high CRI, white light sources require broad and continuous emission across the entire visible spectrum.[104] For a monochromatic HF device, emission arises only from the fluorescent emitter, while for white light, sufficient and well-balanced emission should occur from both TADF and fluorescent molecules (Fig. 6).

White HF-OLEDs can be constructed using a single emissive layer (EML) or multiple emissive layers. Single EML white HF-OLEDs have simple device structures, where white light can be obtained by using the complementary color of the TADF sensitizer and fluorescent emitter. DMAC-DPS was widely used initially for blue emission with conventional emitters rubrene and TBRb as corresponding dopants.[105–107] Wu *et al.* demonstrated a single EML white HF-OLED with DMAC-DPS and TBRb, achieving a maximum EQE of 14.6%.[108] Later, various

new blue TADF materials, such as 2tCz2CzBn (Fig. 7a and b), 3Ph$_2$CzCzBn, and *m*SOAD have been developed for fabricating single EML devices using rubrene and TBRb.[109,113,114] However, it was found that FRET from the TADF to fluorescent dopant becomes more effective than the direct emission from TADF molecules, resulting in poorly balanced white light. Moreover, the blue emission peak in the EL spectra also varied with increasing luminance of the device, indicating unstable color. To overcome these issues, the use of multiple emissive layers or the introduction of interlayers has been suggested.

Multiple emissive layer white HF-OLEDs consisting of more than one emissive layer are known to achieve better efficiency and CRI than single EML white OLEDs. Wu *et al.* fabricated an efficient multi-EML device employing three emissive layers, DMAC-DPS:0.5 wt% DBP, DMAC-DPS:1 wt% DBP:0.5 wt% TTPA and DMAC-DPA:0.2 wt% TTPA and achieved a maximum EQE of 18.2% and a CRI of 82.[115] This sandwich-type emissive structure broadened the recombination region to reduce annihilation processes and ensured adequate blue emission. Another report showed EQE above 20% by carefully selecting emitters and layer thicknesses for blue and yellow EMLs. Here, the triplet state of the blue fluorescent emitter 4P-NPD matched well with the excited states of the green TADF molecule (PXZ-TRZ) used in the yellow EML (TBRb dopant), resulting in high exciton utilization.[116] The performance of multi-EML white HF-OLEDs could also be enhanced by inserting a thin interlayer or spacer layer between the EMLs. Higuchi *et al.* reported an improvement in efficiency from 12.0% to 16.0% by adding a thin *m*CP spacer layer of 2 nm between the two emissive layers (Fig. 7c and d).[110] The interlayer widens and adjusts the exciton recombination zone, preventing direct recombination on the fluorescent dopant. It helps the generated excitons to smoothly transfer to the adjacent layers and tune the color intensity of each EML for a high CRI value.[117] The interlayer between the emissive layers may even be introduced in three-color or four-color white OLEDs (Fig. 7e and f) in order to control the exciton management and thus provide a high CRI and EQE.[111,118] Recently, Liu *et al.* demonstrated an outstanding EQE of 30.8% and a power efficiency of 110.7 lm W^{-1} in a purely organic white OLED based on interlayer sensitization using the sky-blue emitter TCP-BP-SFAC, orange layer 4CzTPNBu and the red fluorescent dopant DBP.[119] The group reported another white OLED showing

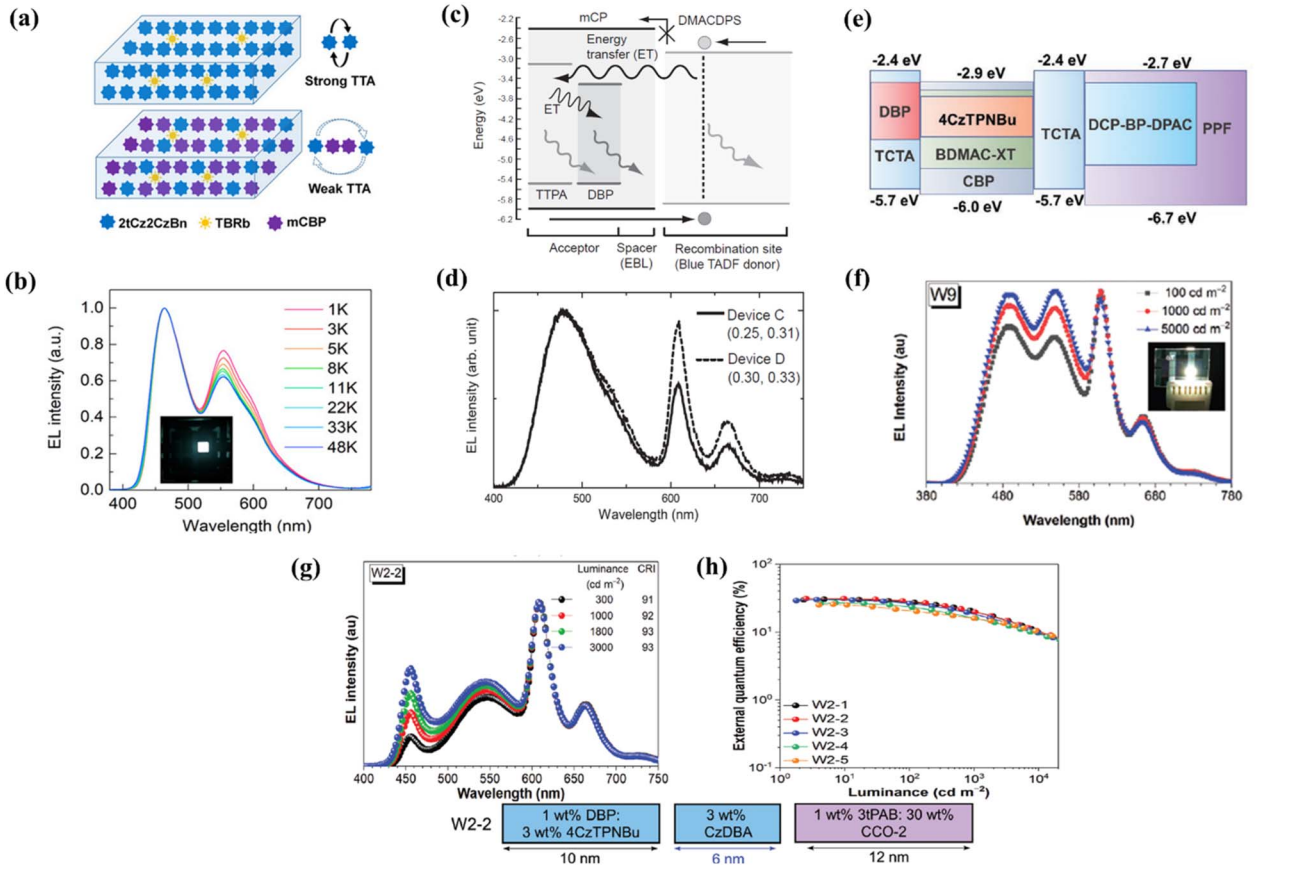

Fig. 7 White hyperfluorescent OLEDs. (a and b) Schematic representation of 2tCz2CzBn:TBRb and *m*CBP:2tCz2CzBn:TBRb in the single emissive layer white OLEDs and electroluminescence spectra at various luminances. Reproduced with permission from ref. 109, American Chemical Society, 2020. (c and d) Schematic illustration of the energy transfer mechanism under electrical excitation with a 2 nm *m*CP emissive layer and electroluminescence spectra of the white device. Reproduced with permission from ref. 110, John Wiley and Sons, 2015. (e and f) Device structure using multiple emissive layers and electroluminescence spectra recorded at different luminances. Reproduced with permission from ref. 111, John Wiley and Sons, 2021. (g and h) Electroluminescence spectra and EQE of white OLEDs based on the interlayer sensitization strategy. Reproduced with permission from ref. 112, John Wiley and Sons, 2023.

Table 2 White hyperfluorescent OLEDs

Emissive layer	EQE_{max}/ 1000 cd m^{-2} (%)	PE_{max}/ 1000 cd m^{-2} (lm W^{-1})	CIE	CRI	Ref.
Single emissive layer					
DMAC-DPS:(0.6%) rubrene	7.48/7.31	15.9/14.7	(0.359, 0.439)	—	105
DPEPO:(50%) DMAC-DPS:(0.03%) TBRb	17.6/14.5	41.0/22.7	(0.23, 0.31)	44.7	106
DPEPO:(50%) DMAC-DPS:(0.05%) TBRb	15.5/13.3	39.3/23.4	(0.28, 0.35)	58.6	106
DPEPO:DMAC-DPS:(0.2%) TBRb	14.6/11.9	51.6/26.9	(0.34, 0.47)	—	108
*m*CBP:(30%) 2tCz2CzBn:(0.2%) TBRb	21.8/14.2	43.9/15.7	(0.292, 0.343)	—	109
*m*SOAD:(0.8%) rubrene	9.8	29.0	(0.30, 0.45)	—	113
*m*CBP:(20%) 3Ph2CzCzBN:(0.5%) TBRb	20.9/13.5	—	(0.31, 0.41)	60	114
*m*CPBC:(10%) 5TCzBN:(1%) TBRb	19.6/15.4	52.2/29.1	(0.33, 0.45)	—	120
Multiple emissive layers					
DMAC DPS:(0.5%) DBP/DMAC-DPS:(1%) DBP:(0.5%) TTPA/ DMAC-DPA:(0.2%) TTPA	18.2/16.2	44.6/27.2	(0.318, 0.390)	82	115
SF4-TPE:(30%) PXZ-TRZ:(1%) TBRb/SF4-TPE:(40%) 4P-NPD	24.5/23.5	65.4/50.8	(0.47, 0.49)	—	116
(1%) DBP:(10%) TTPA:*m*CP/*m*CP (2 nm)/DMAC-DPS	12.1	22.0	(0.25, 0.31)	74	110
(0.4%) TBRb:(6%) 4CzPN/(0.8%) TBRb:(10%) 4CzPN:*m*CBP:(40%) Bepp2:*m*CBP/Bepp2 (3 nm)/ (5%) DSA-Ph:MADN	15.1/12.1	47.4/25.1	(0.35, 0.49)	49	118
(0.4%) DBP:(6%) 4CzPN/(0.8%) TBRb:(10%) 4CzPN:*m*CBP:(40%) Bepp2:*m*CBP/Bepp2 (3 nm)/ (0.3%) DBP:(5%) DSA-Ph:MADN	12.9/10.2	28.2/17.2	(0.42, 0.46)	78	118
TCTA:(1%) DBP/CBP:(30%) BDMAC-XT:(2%) 4CzTPNBu/TCTA (2 nm)/PPF:(20%) DCP-BP-DPAC	22.8/12.0	57.9/24.5	(0.273, 0.408)	73	111
TCTA:(1%) DBP/CBP:(30%) BDMAC-XT:(4%) 4CzTPNBu/TCTA (2 nm)/PPF:(20%) DCP-BP-DPAC	20.3/11.1	56.1/22.8	(0.340, 0.409)	87	111
(1%) DBP:TCP-BP-SFAC/(1.5%) 4CzTPNBu:TCP-BPSFAC/TCP-BP-SFAC	30.8/20.6	106.8/52.6	(0.394, 0.476)	—	119
(1%) DBP:(3%) 4CzTPNBu:DMIC-TRZ/(3%) CzDBA:DMIC-TRZ/(1%) 3tPAB:(30%) CCO-2:*m*CBP	31.0/20.0	80.5/33.6	(0.426, 0.412)	93	112

a comprehensive high EQE of 31.0% and a remarkable CRI of 93 using the interlayer sensitization strategy.[112] The synergistic effect of the adjacent TADF sensitizing layer (3 wt% CzDBA:DMAC-TRZ) combined with a low concentration of the TADF electron capturing agent 4CzTPNBu, co-doped with the red emitter DBP helped in achieving high device performance (Fig. 7g and h). The device performances of different white HF-OLEDs are summarized in Table 2.

4. Approaches to obtain high-performance HF-OLEDs

Obtaining high-performance HF devices is quite challenging as the FRET process is accompanied by competing loss channels. The two main efficiency loss mechanisms under electrical excitation in HF-OLEDs are (i) Dexter energy transfer from the triplet state of the sensitizer to the triplet state of the fluorescent emitter and (ii) direct charge trapping or carrier recombination on the fluorescent dopant. Both processes lead to the formation of triplet excitons on the final fluorescent emitter, from where they decay non-radiatively. These loss mechanisms not only affect efficiency but also the device lifetime since the long-lived triplet states may cause material degradation. Direct charge recombination on the fluorescent emitter can be minimized by doping the final dopant at very low concentrations (<1 wt%) into the emissive layer. Gottardi *et al.* studied the efficiency loss mechanisms in HF-OLEDs using Monte Carlo simulations and discussed the formation of charge-transfer states between the TADF sensitizer and the fluorescent molecule, which can substantially affect the EQE and roll-off characteristics.[121] At lower voltages, the loss process is mainly attributed to the non-radiative triplet states, while at higher voltages, a large contribution arises from various annihilation processes, including singlet–triplet annihilation in the fluorescent emitter. Abroshan *et al.* studied the electronic transitions of a series of fluorescent dopants generally used in HF systems and found that if T_2/T_3 states of the fluorescent emitter are close to the S_1 state, then those triplet states are typically similar in energy to T_1(TADF). Thus, energy losses in the device arise *via* DET from T_1(TADF) to T_2/T_3(fluorescent emitter).[122] The work suggested a design principle for fluorescent dopants with large energy level differences between S_1 and T_2/T_3 to effectively suppress DET. Hence, various strategies to suppress these energy loss processes have been reported and are described in the following.

4.1 Molecules with peripheral inert substitution

DET can be considered as the key loss process in HF-OLEDs.[40] A fast RISC rate of the TADF sensitizer helps to reduce the triplet exciton density, hence controlling this loss process.[123] Along with accelerated RISC, the intermolecular distance between the

TADF sensitizer and the final fluorescent dopant plays a crucial role in minimizing DET. Fortunately, DET is a short-range energy transfer (~1 nm), and the process can be effectively inhibited by increasing the distance between TADF and fluorescent molecules.[20,124,125] One way to increase the intermolecular distance is through inserting electronically inert peripheral substitutions in the emitter (Fig. 8a) (either in the TADF sensitizer or in the fluorescent emitter or in both). Such bulky substitutions electronically shield the active core of the emitter, hindering orbital overlap and effectively managing DET by preventing intermolecular interactions between the sensitizer and the emitter (Fig. 8b).[64] Zhang *et al.* observed the highest efficiency for PhtBuPAD-based HF devices, which have a bulky group in the molecular structure, among the series of PAD green emitters. The addition of the bulky unit in the final dopant proved to be efficacious in achieving high EQE and low roll-off by suppressing the energy loss paths from the TADF sensitizer to the final emitter.[64,127] Xie *et al.* introduced an inert phenylfluorene unit onto the donor moiety of the TADF sensitizer to block energy loss pathways in HF-OLEDs.[72] Molecular dynamics simulation results showed that the intermolecular distance between the molecules increased by 0.7 Å after adding the bulky group, which effectively decreased the DET rate and achieved a maximum EQE of 18.1% for red HF-OLEDs with narrow emission. Alam *et al.* reported a deep-blue emitter, KCTBC, with a twisted interlocked acceptor core framework, which showed an EQE of 13.9% with the sensitizer 4CzFCN.[128] Bartkowski *et al.* introduced a new rational design by rigidifying the TADF sensitizer with π-extension conjugation and demonstrated a yellow HF-OLED showing an excellent EQE of 27% with narrowband emission (FWHM = 40 nm).[129] Lee *et al.* very recently reported TADF emitters with isonicotinonitrile as the acceptor and benzothienocarbazole as the donor to create bulkiness in the molecules which can effectively block DET from the TADF sensitizer to the red fluorescent dopant DBP.[73] The molecules suppressed DET, accelerated the RISC process, and achieved an EQE of 14.7% for red HF-OLEDs (Fig. 8c and d). Wei *et al.* reported single EML white HF-OLEDs with sterically shielded TADF emitters and fluorescent dopants, to modulate FRET and DET and achieved good electroluminescence performance.[120] The electronically shielded peripheral units not only blocked DET to prevent triplet exciton quenching but also suppressed the FRET rate to the fluorescent dopant. Hence, they could retain the blue emission intensity from the TADF emitter for balanced white light.

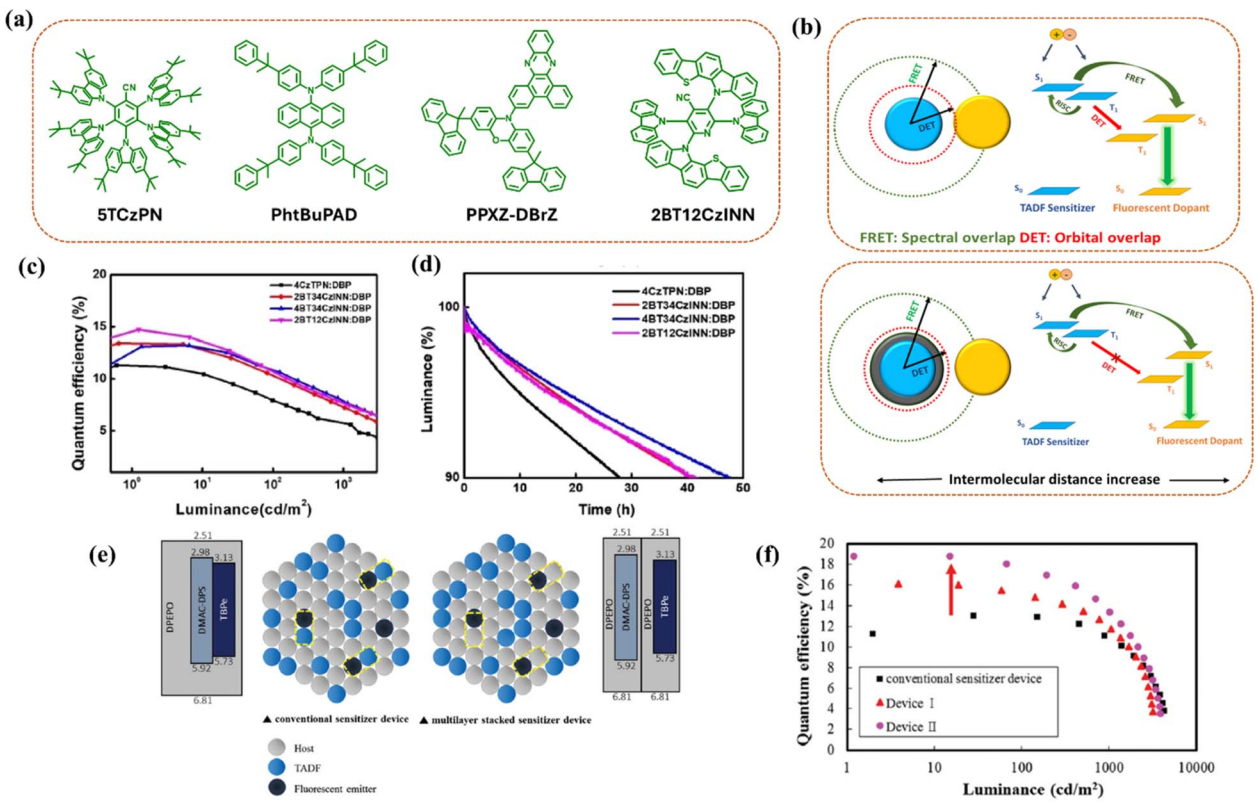

Fig. 8 Peripheral inert substitution. (a) Molecular structures of emitters with bulky blocking peripheral units. (b) A schematic diagram of FRET and DET on intermolecular distances between the TADF sensitizer and the final fluorescent dopant along with the energy transfer processes without peripheral inert units (top) and with peripheral inert units (bottom). The blue and yellow spheroids represent the TADF sensitizer and fluorescent emitter, respectively, and the gray spheroid indicates the peripheral inert unit. (c and d) Efficiency *vs.* luminance plots and device lifetime of the HF-OLEDs based on TADF sensitizers with bulky blocking substitutions. Reproduced with permission from ref. 73, American Chemical Society, 2023. (e and f) Schematic illustration to manage Dexter energy transfer and quantum efficiency *vs.* luminance plots of the respective devices. Reproduced with permission from ref. 126, Royal Society of Chemistry, 2018.

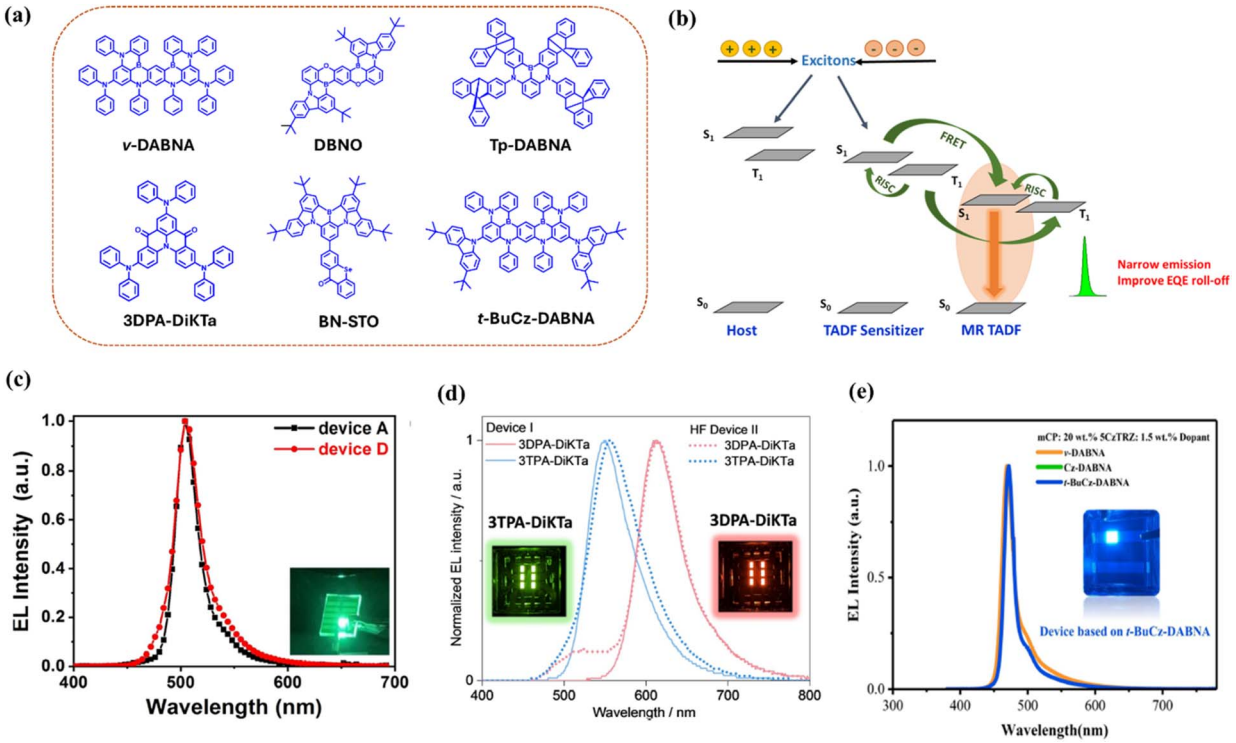

Fig. 9 MR-TADF emitters as the final dopant. (a) Molecular structures of MR-TADF emitters. (b) A schematic diagram of the hyperfluorescent energy transfer mechanism for MR-TADF as the final dopant. (c) Electroluminescence spectra of DBNO-based green HF-OLEDs. Reproduced with permission from ref. 139, John Wiley and Sons, 2022. (d) Electroluminescence spectra of TADF and HF devices based on green and red MR-TADF molecules with a DiKTa acceptor core. Reproduced with permission from ref. 140, John Wiley and Sons, 2022. (e) Electroluminescence spectra of solution-processed blue HF devices based on *t*-BuCz-DABNA. Reproduced with permission from ref. 141, John Wiley and Sons, 2023.

Separating the molecules of TADF and the final dopant by inserting bulky blocking units seems to be an effective way to modulate the energy transfer mechanism in HF-OLEDs. Another way to manage DET is by constructing a multilayer emitting structure by spatially separating the sensitizer layer and the fluorescent emitter layer to confine all excitons similar to a quantum well structure.[130,131] With the help of device engineering, Han *et al.* reported an improved efficiency from 13.1% to 18.8% by using simple molecules without any rigid unit (Fig. 8e and f).[126] Jakoby *et al.* investigated the effect of singlet and triplet exciton diffusion lengths of TADF molecules in HF systems using Monte Carlo simulations.[132] Since the concentration of the final emitter needs to be kept low, most of the excitons diffuse between the TADF molecules before reaching the final dopant. The work suggested two ways to improve HF efficiency: first, to incorporate steric protection in the emitter, as an unprotected emitter would increase the triplet motion and second, to develop TADF molecules with shorter triplet diffusion lengths as it could restrict triplet transport between the molecules.

4.2 Multi-resonant (MR) TADF emitters as final dopants

Lately, the development of organo-boron-based TADF dopants has caught attention due to their multi-resonance (MR) effect between boron and nitrogen (or oxygen) atoms which can minimize vibronic coupling and thus reduce the singlet–triplet energy gap (ΔE_{ST}).[133] The electron-deficient boron and electron-rich nitrogen atoms were inserted into rigid polycyclic aromatic rings (DABNA-1 and DABNA-2).[134] The boron and nitrogen atoms were placed in such a way that they induced an opposite resonance effect/multi-resonance character in the molecule. In this unique molecular design, unlike conventional TADF emitters, FMOs were distributed over the atoms with LUMOs on boron and carbon adjacent to nitrogen and HOMOs on nitrogen and carbon adjacent to boron. This atomic separation of FMOs leads to a small ΔE_{ST}, large oscillator strength, and narrow emission (FWHM $\leq$25 nm).[135–138] This class of emitters is called MR-TADF emitters (Fig. 9a) and may achieve high efficiency in TADF OLEDs without compromising on the color purity of the emission.

Regardless of these benefits, MR-TADF emitters typically suffer from severe efficiency roll-off at high current density as the RISC rates of MR-TADF compounds are often lower due to the long triplet lifetime, which leads to increased roll-off.[142] This limitation of MR-TADF materials can be overcome by utilizing them as final dopants in HF systems (Fig. 9b). In combination with an efficient TADF sensitizer, HF-OLEDs based on narrow-band MR-TADF final dopants represent a promising approach for practical applications in commercial displays.

Kondo *et al.* reported the efficient organo-boron-based TADF emitter *v*-DABNA (ΔE_{ST} = 0.017 eV) featuring rigid benzene rings that are connected by boron and nitrogen atoms.[143] The

device exhibited the multiple resonance effect of boron and nitrogen atoms, which gave rise to an extremely sharp blue emission at 468 nm with a FWHM of 18 nm and a maximum EQE of 34.4%. These advantages of *ν*-DABNA look promising and can be implemented to expand its properties in fabricating high-efficiency HF-OLEDs. Chan *et al.* developed a strategy to obtain high-performance deep-blue OLEDs by efficiently transferring exciton energy from the TADF sensitizer TPh2Cz2DPhCzBN (HDT-1) to the singlet state of narrow emitter *ν*-DABNA.[144] The device showed a maximum EQE of 27% and retained an EQE of 20% even at a high luminance of 1000 cd m^{-2}. Furthermore, to boost the performance of the device, a two-unit stacked tandem HF-OLED was designed, achieving a maximum EQE of 41% and 32% at 1000 cd m^{-2} along with deep-blue and narrow emission. Mamada *et al.* also utilized the benefits of *ν*-DABNA as a final dopant after carefully screening different D–A structure-based TADF sensitizers with benzonitrile and carbazole rings.145 The blue HF-OLED exhibited a maximum EQE of 22.4% with a reduced roll-off of 17.8% at 1000 cd m^{-2}. Very recently, Lee *et al.* demonstrated a quadrupolar D–A–D type TADF sensitizer, DBA-DTMCz, which exhibited an outstanding EQE_{max} of 43.9% with the *ν*-DABNA emitter.[146] The device maintained its high EQE of 37.5% even at 1000 cd m^{-2}, indicating low-efficiency roll-off due to suppressed DET. Han *et al.* reported a pure blue HF-OLED using a derivative of the DABNA family, a fused B–N emitter, *t*DABNA, which showed a high EQE of 31.4%, with DMAC-DPS as a sensitizer.[147] Mubarok *et al.* proposed a bulky, sterically shielded triptycene-fused deep-blue MR-TADF emitter, Tp-DABNA, where the rigid units can suppress the DET process and help in improving the device performance while maintaining narrow emission (26 nm).[148] The HF-OLED based on Tp-DABNA and sensitizer TDBA-SAF demonstrated an EQE of 28.7%.

Another MR-TADF emitter, α-3BNMes, based on a B–N heptacene core with CIE_y <0.1 was utilized as the final dopant, achieving a deep-blue HF-OLED with an EQE of 15%.[149] The color coordinates reported were one of the lowest for deep-blue HF-OLEDs. Cai *et al.* reported a B–O–N-embedded MR-TADF emitter, DBNO, which showed narrowband green emission (Fig. 9c) and demonstrated high horizontal molecular orientation (96%).[139] The DBNO-based OLED showed an EQE above 30% but experienced serious roll-off at high brightness. However, the DBNO-based HF-OLED obtained a high EQE_{max} of 37.1%, retaining up to 20.6% at 1000 cd m^{-2} with a FWHM of 27 nm. Hu *et al.* proposed a green MR-TADF emitter, BN-STO, decorated with peripheral heavy-atom selenium integration showing a high EQE of 40.1% and high color purity (FWHM = 29 nm, $CIE_y = 0.70$).[150] Using the sky-blue sensitizer, 5TBuCzBN, the maximum EQE of the HF-OLED obtained with BN-STO is 39.8% while exhibiting reduced efficiency roll-off, with an EQE of 34.0% at 1000 cd m^{-2} and 23.4% at 5000 cd m^{-2}. Furthermore, Wu *et al.* demonstrated green and red MR-TADF molecules with a DiKTa acceptor core showing excellent EL performance (Fig. 9d).[140] The maximum EQE obtained for the green HF-OLED was 30%, and for the red HF-OLED was 17.9%, also featuring reduced roll-off at high luminance. In a recent report, Stavrou *et al.* described the impact of the molecular structure of the sensitizer on FRET efficiency to obtain efficient HF-OLEDs.[151] The work utilized a contrasting green sensitizer, ACRSA, to assist the blue MR-TADF emitter *ν*-DABNA and obtained a maximum EQE of 28.5%, while a pure ACRSA-based TADF OLED showed a low EQE of 11.0% with high roll-off due to longer exciton lifetime. The work suggested a sensitization process where long-excited state lifetime TADF emitters could facilitate efficient FRET while maintaining balanced rate constants to ensure device stability.

Currently, achieving efficient solution-processed HF devices remains a significant challenge. For instance, Zhang *et al.* developed the MR-TADF emitter *t*-BuCz-DABNA, which has a low-lying HOMO level. Here, the peripheral carbazole unit in

Table 3 Hyperfluorescent OLEDs with MR-TADF emitters as final dopants

Final dopant	Sensitizer	Host	EL (nm)	FWHM (nm)	EQE_{max}/ 1000 cd m^{-2} (%)	PE_{max}/ 1000 cd m^{-2} (lm W^{-1})	CIE	Ref.
ν-DABNA	TPh2Cz2DPhCzBN (HDT-1)	*m*CBP	470	18	27/20	41/16	(0.15, 0.20)	144
ν-DABNA	4PhCz2BN	*m*CBP	470	18	22.4/17.8	25/9.4	(0.13, 0.15)	145
ν-DABNA	DBA-DTMCz	DBFPO	473	21	43.9/37.5	—	(0.12, 0.16)	146
t-DABNA	DMAC-DPS	DPEPO		31	31.4/19.8	—	(0.13, 0.15)	147
Tp-DABNA	TDBA-SAF	DPEPO	462	29	28.7/—	29.8/-	(0.14, 0.13)	148
α-3BNMes	DtBuAc-DBT	DPEPO	442	49	15/—	—	(0.15, 0.10)	149
DBNO	5TCzBN	PhCzBCz	504	27	37.1/20.6	105.6/—	(0.14, 0.53)	139
BN-STO	5TBuCzBN	DMIC-TRZ	511	32	39.8/34.0	138.4/—	(0.15, 0.66)	150
3TPA-DiKTa	4CzIPN	*m*CP	556	70	30.0/20.0	111/—	(0.42, 0.55)	140
3DPA-DikTa	4CzIPN	*m*CP	615	61	17.9/6.0	37/—	(0.58, 0.39)	140
ν-DABNA	ACRSA	*m*CBPCN	473	19	28.5/18.6	36/12	(0.13, 0.17)	151
ν-DABNA	PPCzTrz-	*o*CBP:CNmCBPCN	473	24	33.0/25.2	—	(0.13, 0.20)	152
ν-DABNA	PCzTrz	*o*CBP:CNmCBPCN	473	29	33.5/23.8	—	(0.12, 0.18)	152
Solution-processed HF-OLEDs								
t-BuCz-DABNA	5CzTRZ	*m*CP	472	16.6	29.2/26.0	33.9/19.0	(0.13, 0.18)	141

the emitter suppressed molecular aggregation and improved solubility. The emitter was utilized to fabricate solution-processed HF-OLEDs (sensitizer: 5CzTRZ) (Fig. 9e) that achieved a maximum EQE of 29.2% and 26.0% at 1000 cd m^{-2}, which is one of the best results reported for solution-processed HF-OLEDs.[141] The performances of HF-OLEDs using MR-TADF emitters as final dopants are presented in Table 3.

4.3 Exciplex-sensitized HF-OLEDs

Another approach for harvesting both singlet and triplet excitons in HF-OLEDs is the use of exciplex-based co-host systems (Fig. 10a) with subsequent exciton transfer *via* FRET to the fluorescent emitter (Fig. 10b). Exciplexes form between two dissimilar molecules possessing different energy levels by resonance interaction or charge transfer. Such a co-host system containing donor- and acceptor-type molecules (Fig. 10c) can outperform traditional hosts in terms of operating voltage, efficiency roll-off and device lifetime.[155–157] Exciplex hosts can exhibit TADF characteristics due to their inherent donor–acceptor-type structure, which reduces the exchange energy and hence leads to small ΔE_{ST}. However, the participating materials need to be selected carefully in order to ensure that the triplet levels of the two individual host molecules are higher than the triplet energy of the exciplex.[156] Moreover, for exciplex to show TADF features, the HOMO and LUMO offsets between the donor and acceptor materials should be sufficiently large to ensure enough charge accumulation at the donor–acceptor interface.[157,158]

Liu *et al.* demonstrated an exciplex co-host system with the TADF effect based on the blend TAPC:DPTPCz, where TAPC was the donor, and DPTPCz was the acceptor material. They used this co-host to sensitize the fluorescent emitter C545T, achieving an EQE of 14.5%.[159] Another TADF type exciplex host TCTA:B4PyMPM has been explored by Kim and co-workers which has close to 0 eV ΔE_{ST}, indicating a fast RISC process.[160] This green-emissive exciplex efficiently transferred energy to the red fluorescent emitter DCJTB and realized an EQE of 10.6%. Similar results for DCJTB in HF-OLEDs have also been obtained using the exciplex hosts TCTA:3PT2T and tris-PCz:CNT2T.[161,162] Nguyen *et al.* utilized a TADF-type electron acceptor with a triazine derivative, 3Cz-TRZ, which formed an exciplex with tris-PCz and showed an EQE of around 10%.[163] The performance improved two-fold (EQE ~19%) when it was used as a co-host to sensitize *v*-DABNA.

Liang *et al.* introduced a high triplet energy electron acceptor based on benzimidazole-triazine, PIM-TRZ, which formed exciplexes with the electron donor TAPC.[164] The pure exciplex device exhibited a low turn-on voltage of 2.3 eV and obtained an EQE of 21.7%. Using TAPC:PIM-TRZ as the co-host for the fluorescent emitter C545T, the maximum EQE was 20.2%, with 18.4% of EQE being retained at 1000 cd m^{-2}, showing significantly reduced roll-off. Li *et al.* fabricated OLEDs with an EQE of

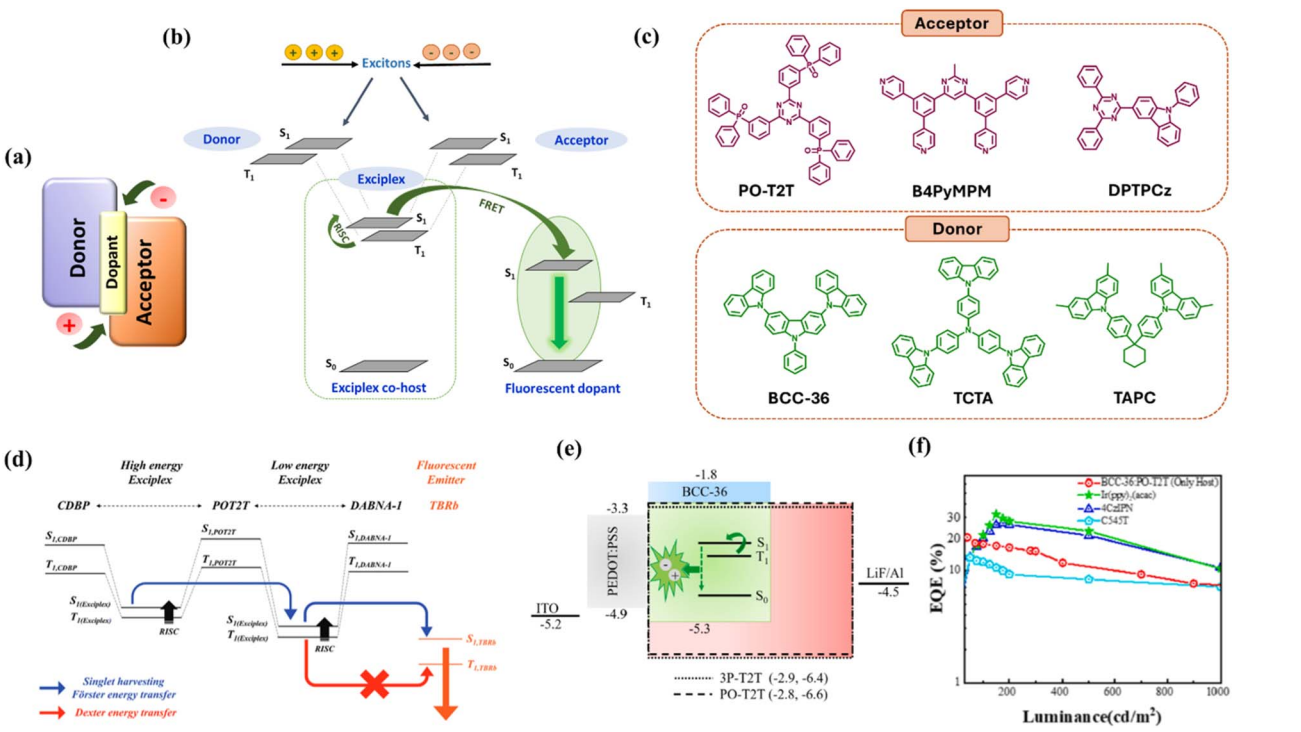

Fig. 10 Exciplex co-host system. (a) A schematic diagram of an exciplex co-host system forming at the interface and a fluorescent dopant. (b) A schematic representation of the energy transfer from an exciplex co-host to a fluorescent dopant. (c) Molecular structures of donor and acceptor materials used to form exciplex hosts. (d) The cascade singlet harvesting mechanism using a high-energy exciplex and a low-energy exciplex to sensitize a fluorescent emitter. Reproduced with permission from ref. 153, John Wiley and Sons, 2020. (e and f) The device structure of an exciplex OLED and EQE *vs.* luminance plots of the exciplex device and sensitized OLEDs. Reproduced with permission from ref. 154, Elsevier, 2022.

Table 4 Exciplex sensitized hyperfluorescent OLEDs

Final dopant	Exciplex co-host	EQE_{max}/1000 cd m^{-2} (%)	PE_{max}/1000 cd m^{-2} (lm W^{-1})	CIE	Ref.
(0.2%) C545T	TAPC:DPTPCz	14.5	46.1	(0.24, 0.55)	159
(0.5%) DCJTB	TCTA:B4PYMPM	10.6	26.8	—	160
(1.0%) DCJTB	TCTA:3P-T2T	10.15/10.03	21.5/18.9	—	161
(1.0%) DCJTB	Tris-PCz:CN-T2T	9.7/9.1	23.3	(0.59, 0.40)	162
(1.0%) *ν*-DABNA	Tri-PCz:3Cz-TRZ	19/18	—	—	163
(0.6%) C545T	TAPC:PIM-TRZ	20.2/18.4	86.4/51.1	(0.29, 0.64)	164
(0.5%) DCJTB	TCTA:B4PYMPM:4CzIPN	12.9/10.1	24.0/12.7	(0.58, 0.41)	165
(0.5%) TBRb	CDBP:POT2T:DABNA-1	18.7/18.0	46.7/36.0	(0.41, 0.56)	153
(0.5%) TBRb	CDBP:POT2T:*t*-DABNA	19.9	—	(0.45, 0.53)	153
Solution-processed HF-OLEDs					
(0.5%) DCJTB	TCTA:PO-T2T	8.1	11.1	(0.52, 0.46)	166
(1.0%) C545T	BCC36:POT2T	12.5/7.1	25/14.6	(0.24, 0.57)	154
(7.5%) 4CzIPN	BCC36:POT2T	26.5/10.6	39.1/27.2	(0.26, 0.56)	154

12.9% based on a double sensitizer system which deployed an exciplex co-host, TCTA:B4PyMPM, and the TADF molecule 4CzIPN acting as an additional sensitizer for the red fluorescent emitter DCJTB.[165] Further improvement can be achieved using a cascade energy transfer *via* two TADF-type exciplexes to selectively transfer singlet excitons to the fluorescent emitter. Following this strategy, Lee *et al.* used CDBP:PO-T2T as a high-energy exciplex and PO-T2T:*t*-DABNA as a low-energy exciplex to enable efficient FRET to the fluorescent emitter TBRb (Fig. 10d) and obtained an EQE of 19.9%.[153] Wang *et al.* fabricated solution-processed red fluorescent OLEDs using a diluted exciplex host, TCTA:PO-T2T, to reduce non-radiative triplet exciton loss and obtained an EQE_{max} of 8.1% for DCJTB.[166] Kesavan *et al.* reported a solution-processed OLED with an EQE above 25% for the TADF exciplex BCC-36:PO-T2T which has been used as a co-host to sensitize the TADF emitter 4CzIPN (Fig. 10e and f).[154] To conclude, sensitization of singlet excitons *via* TADF-type exciplex co-hosts offers an efficient alternative to conventional TADF assistant dopants in realizing efficient HF-OLEDs. However, achieving exciplex co-hosts for blue fluorescent dopants has been challenging as they require an extremely large energy gap in order to sensitize the blue emitters. The device performances of exciplex-sensitized HF-OLEDs are summarized in Table 4.

5. Status of operational lifetime

The long operational lifetime of OLEDs is one of the key requirements for commercial applications. Despite high EQE, the device lifetime for TADF-based OLEDs is low as compared to traditional fluorescent OLEDs[167–169] due to the presence of long-lived excitons in triplet states, which lead to material degradation and short operational lifetime.[170–172] Here, hyperfluorescent systems, which contain both TADF and fluorescent emitters, could offer prospects for realizing high efficiency and stability in OLEDs due to reduced excited state lifetime in the overall emission process and material stability of fluorescent dopants. For example, Furukawa *et al.* reported a yellow HF device in 2015 with 4CzIPN-Me as the TADF sensitizer and TBRb as the fluorescent emitter showing an operational lifetime LT_{50} of 3775 h at 1000 cd m^{-2}, which was over two times longer than that of the conventional TADF-based device.[74] However, in HF-OLEDs, the presence of triplet excitons on the TADF sensitizer results in accelerated degradation of the devices. These particularly long-lived excitons participate in various annihilation processes inside the device, such as singlet–triplet annihilation, triplet–triplet annihilation, and triplet–polaron annihilation, which accelerate the loss mechanism.[173,174] Therefore, the management of these exciton loss processes is important to ensure a long lifetime in HF devices.

There are some factors which can be employed to improve the operational lifetime of HF-OLEDs. First, the TADF assistant dopant should possess a fast RISC rate, as well as a high bond dissociation energy (BDE). TADF molecules with low BDE hinder the stability of the device and lead to a shorter operational lifetime. Typically, the BDE of the TADF emitters should be higher than their exciton energy.[175] In addition to stable TADF emitters, the host material and all charge-transporting layers in the multilayer structure must also exhibit high BDE to extend the device's overall durability.[176] Second, the diffusion of triplet excitons from TADF to the final dopant should be minimized, which is possible by introducing bulky unit groups in the TADF sensitizer or in the final dopant. Third, the device structure needs to be optimized for a longer lifetime since OLEDs consist of a multilayer structure, in which each layer contributes to the overall performance and stability of the device. Here, appropriate charge transporting and exciton blocking layers need to be selected in combination with the respective emissive layer. Stacking of devices can improve the lifetime as reported by Chan *et al.*, who showed that a two-unit stacked tandem HF-OLED with *ν*-DABNA can increase the operational lifetime from an LT_{95} of 11 h at 1000 cd m^{-2} for the single unit to 18 h in the double unit (Fig. 11a and b).[144] Nakamura *et al.* reported green HF-OLEDs with a BODIPY emitter, *t*PhBODIPY, as the final dopant in which they achieved an enhancement in the device lifetime from an LT_{50} of 8283 h to 14 443 h at 1000 cd m^{-2} by using three stacked hole transporting layers (HTLs) (Fig. 11c).[67] Since charge accumulation at

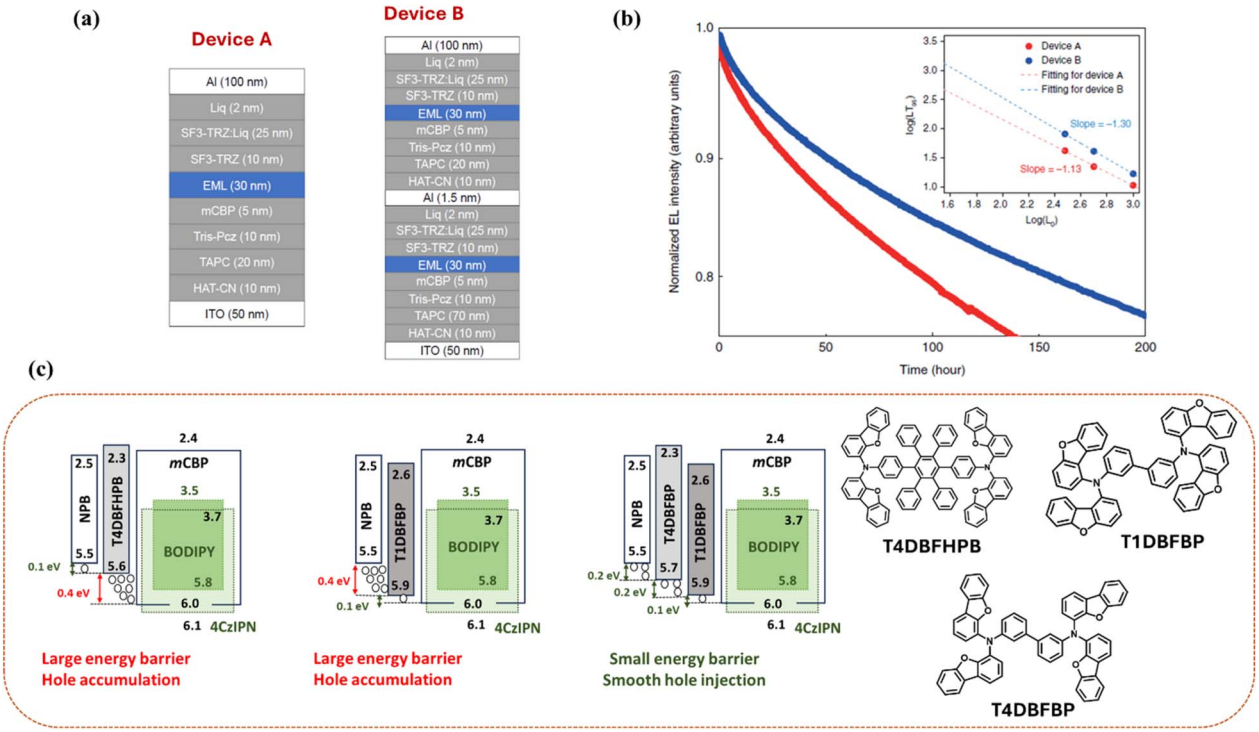

Fig. 11 (a) Device structure of single-unit and two-unit stacked tandem hyperfluorescent OLEDs. (b) Electroluminescence intensity *versus* operation time at an initial luminance of 1000 cd m^{-2}. Inset: LT_{95} as a function of L_0. Reproduced with permission from ref. 144, *Nature*, 2021. (c) Schematic illustration of hole injection behaviour from the HTL to the EML using various HTLs, along with the molecular structures of the respective HTLs used.

interfaces is detrimental to device stability,[177,178] the improved energy alignment in the triple HTL structure helped reduce hole trapping at the HTL/EML interface, resulting in an enhanced lifetime.

Kim *et al.* reported a yellow TADF sensitizer with a strong bulky donor, 5,10-diphenyl-10,15-dihydro-5*H*-diindolo carbazole (TruX), having a distorted geometry from the linker plane. The HF device utilized TBRb as the final dopant and demonstrated a device lifetime LT_{90} of 1400 h at 1000 cd m^{-2}.[75] The extended lifetime in the device indicated efficient FRET due to the high RISC rate of the sensitizer, which reduced the long-delayed component and suppressed the triplet exciton population in the device. Lee *et al.* reported the bulky, high-RISC rate TADF sensitizer 2BT34CzINN to fabricate HF-OLEDs with DBP and achieved a device lifetime LT_{90} of 40 h at 3000 cd m^{-2}.[73] Shin *et al.* mentioned an operational lifetime LT_{90} of 1312 h at 3000 cd m^{-2} for a red HF-OLED with 12BTCzTPN as the TADF sensitizer and 4tBuMB as the final dopant.[71] This is one of the longest lifetimes reported for red HF devices. Achieving high EQE and long lifetime simultaneously in blue OLEDs is challenging. Jeon *et al.* reported a high EQE of over 30% and a long lifetime LT_{50} of over 5000 h (at 100 cd m^{-2}) for a deep-blue (CIE_y <0.10) HF-OLED through triplet exciton recycling using PPCzTrz as the sensitizer with *ν*-DABNA as the final dopant.[152] Until now, yellow HF-OLEDs have already been commercialized in small display applications such as passive matrix OLED displays, while red and green devices have started showing good results and may be implemented in commercial products shortly.[179,180] However, blue HF devices, still require significant optimization to obtain both high efficiency and stability to enter the commercial market.

6. Summary and outlook

In summary, hyperfluorescent OLEDs have shown great potential in achieving high efficiency, good color saturation and a long device operational lifetime, which paves the way for their implementation in practical applications. Efficient emitters are essential for high-performance devices, together with finely tuned molecular distances and energy levels of the TADF sensitizer and final emitter in order to improve device efficiency and roll-off characteristics. FRET between the TADF sensitizer and the final dopant is the primary energy transfer process in the HF-OLEDs; hence, sufficient spectral overlap between the emitters is important to increase the energy transfer efficiency. An efficient FRET process plays a vital role in enhancing the device efficiency for blue, green and red devices, whereas white HF-OLEDs require a well-balanced emission from both TADF and final emitters. Therefore, appropriate material selection and combination are crucial for achieving better device performance. HF-OLEDs are recognized as next-generation efficient devices with pure organic molecules, yet certain challenges must be addressed to fully harness their potential for commercialization.

One of the key challenges in HF-OLEDs is to control the loss mechanisms associated with the energy transfer process. Direct charge trapping on the fluorescent emitter can be reduced by minimizing the doping concentration in the emissive layer, thus preventing the formation of non-radiative triplet excitons. Another energy loss process arises due to DET of triplet excitons from the TADF sensitizer to the fluorescent dopant. DET can be strategically managed by increasing the intermolecular distance between the sensitizer and final dopant *via* inserting electronically inert bulky substitutions in the emitters. Using MR-TADF molecules as final dopants can be advantageous as these can also employ DET for maximum exciton utilization. Furthermore, MR-TADF emitters offer a narrowband spectrum and provide improved EQE roll-off properties in HF-OLEDs. Another approach for realizing efficient devices is using exciplex-sensitized co-host systems. For blue OLEDs, however, only very few exciplex co-hosts are available due to the very high triplet energy gap requirement.

The most critical issue of HF-OLEDs that currently limits their commercialization is the device operational lifetime, particularly for blue HF devices. Although there are several reports on extended operational lifetime, HF-OLEDs still exhibit shorter lifespans as compared to conventional fluorescent devices. The degradation of HF-OLEDs is mainly attributed to the presence of long-lived triplet excitons in the emissive layer, which take part in various annihilation processes. These processes are lethal to the organic layers in the device and, therefore, affect device stability. Hence, the design of the TADF sensitizer is important, emphasizing high BDE and providing a short-delayed fluorescence excited state lifetime while maintaining a stable triplet excited state density for high-efficiency HF devices. With such a robust molecular design and advanced device engineering, HF-OLEDs hold the potential to mitigate the remaining challenges and significantly improve both efficiency and operational lifetime.

Data availability

It is perspective and data availability is not applicable for this submission.

Author contributions

The project was conceptualized by P. R. and U. D. The manuscript was written by U. D. and G. P. N. contributed in the formatting manuscript under supervision C. M. and P. R.

Conflicts of interest

There are no conflicts to declare.

Acknowledgements

The authors thank IISc and the Science & Engineering Research Board (SERB), India, SERB-Power Grant (SPG) (Grant No. SPG/2020/000107) for financial support and The Indo-German Science & Technology Centre (IGSTC) for the WISER award (IGSTC/WISER 2022/RG/52/2022-23) and financial support. The authors thank the German BMBF (13XP5137) and the Deutsche Forschungsgemeinschaft (DFG, German research foundation) through GRK 2767 (451785257) for funding. This work was co-financed by tax revenue based on the budget approved by the Saxon State Parliament.

References

1 C. W. Tang and S. A. VanSlyke, *Appl. Phys. Lett.*, 1987, **51**, 913–915.
2 Y. Sun, N. C. Giebink, H. Kanno, B. Ma, M. E. Thompson and S. R. Forrest, *Nature*, 2006, **440**, 908–912.
3 S. Reineke, F. Lindner, G. Schwartz, N. Seidler, K. Walzer, B. Lüssem and K. Leo, *Nature*, 2009, **459**, 234–238.
4 X. Cai and S.-J. Su, *Adv. Funct. Mater.*, 2018, **28**, 1802558.
5 M. Pope and C. E. Swenberg, *Electronic Processes in Organic Crystals and Polymers*, Oxford University PressNew, York, NY, 1999.
6 A. R. Brown, K. Pichler, N. C. Greenham, D. D. C. Bradley, R. H. Friend and A. B. Holmes, *Chem. Phys. Lett.*, 1993, **210**, 61–66.
7 R. H. Friend, R. W. Gymer, A. B. Holmes, J. H. Burroughes, R. N. Marks, C. Taliani, D. D. C. Bradley, D. A. Dos Santos, J. L. Brédas, M. Lögdlund and W. R. Salaneck, *Nature*, 1999, **397**, 121–128.
8 A. R. Brown, D. D. C. Bradley, J. H. Burroughes, R. H. Friend, N. C. Greenham, P. L. Burn, A. B. Holmes and A. Kraft, *Appl. Phys. Lett.*, 1992, **61**, 2793–2795.
9 H.-H. Chou, Y.-H. Chen, H.-P. Hsu, W.-H. Chang, Y.-H. Chen and C.-H. Cheng, *Adv. Mater.*, 2012, **24**, 5867–5871.
10 H. Jung, S. Kang, H. Lee, Y.-J. Yu, J. H. Jeong, J. Song, Y. Jeon and J. Park, *ACS Appl. Mater. Interfaces*, 2018, **10**, 30022–30028.
11 Y. Zhang and S. R. Forrest, *Phys. Rev. Lett.*, 2012, **108**, 267404.
12 T. Tsutsui, E. Aminaka, C. P. Lin and D.-U. Kim, *Philos. Trans. R. Soc. London, Ser. A*, 1997, **355**, 801–814.
13 S. Nowy, B. C. Krummacher, J. Frischeisen, N. A. Reinke and W. Brütting, *J. Appl. Phys.*, 2008, **104**, 123109.
14 M. Furno, R. Meerheim, S. Hofmann, B. Lüssem and K. Leo, *Phys. Rev. B: Condens. Matter Mater. Phys.*, 2012, **85**, 115205.
15 B. Sim, C.-K. Moon, K.-H. Kim and J.-J. Kim, *ACS Appl. Mater. Interfaces*, 2016, **8**, 33010–33018.
16 M. A. Baldo, D. F. O'Brien, Y. You, A. Shoustikov, S. Sibley, M. E. Thompson and S. R. Forrest, *Nature*, 1998, **395**, 151–154.
17 S. Reineke, T. C. Rosenow, B. Lüssem and K. Leo, *Adv. Mater.*, 2010, **22**, 3189–3193.
18 H. Sasabe and J. Kido, *Eur. J. Org. Chem.*, 2013, **2013**, 7653–7663.
19 C. Fan, L. Zhu, T. Liu, B. Jiang, D. Ma, J. Qin and C. Yang, *Angew. Chem.*, 2014, **126**, 2179–2183.
20 M. A. Baldo, M. E. Thompson and S. R. Forrest, *Nature*, 2000, **403**, 750–753.

21 B. Minaev, G. Baryshnikov and H. Agren, *Phys. Chem. Chem. Phys.*, 2014, **16**, 1719–1758.
22 G. Schwartz, S. Reineke, T. C. Rosenow, K. Walzer and K. Leo, *Adv. Funct. Mater.*, 2009, **19**, 1319–1333.
23 J. Lee, H.-F. Chen, T. Batagoda, C. Coburn, P. I. Djurovich, M. E. Thompson and S. R. Forrest, *Nat. Mater.*, 2016, **15**, 92–98.
24 H. Uoyama, K. Goushi, K. Shizu, H. Nomura and C. Adachi, *Nature*, 2012, **492**, 234–238.
25 H. Kaji, H. Suzuki, T. Fukushima, K. Shizu, K. Suzuki, S. Kubo, T. Komino, H. Oiwa, F. Suzuki, A. Wakamiya, Y. Murata and C. Adachi, *Nat. Commun.*, 2015, **6**, 8476.
26 Z. Yang, Z. Mao, Z. Xie, Y. Zhang, S. Liu, J. Zhao, J. Xu, Z. Chi and M. P. Aldred, *Chem. Soc. Rev.*, 2017, **46**, 915–1016.
27 M. Y. Wong and E. Zysman-Colman, *Adv. Mater.*, 2017, **29**, 1605444.
28 T. J. Penfold, F. B. Dias and A. P. Monkman, *Chem. Commun.*, 2018, **54**, 3926–3935.
29 P. Jiang, J. Miao, X. Cao, H. Xia, K. Pan, T. Hua, X. Lv, Z. Huang, Y. Zou and C. Yang, *Adv. Mater.*, 2022, **34**, 2106954.
30 W. Yang, J. Miao, F. Hu, Y. Zou, C. Zhong, S. Gong and C. Yang, *Adv. Funct. Mater.*, 2023, **33**, 2213056.
31 F. B. Dias, T. J. Penfold and A. P. Monkman, *Methods Appl. Fluoresc.*, 2017, **5**, 012001.
32 Q. Zhang, J. Li, K. Shizu, S. Huang, S. Hirata, H. Miyazaki and C. Adachi, *J. Am. Chem. Soc.*, 2012, **134**, 14706–14709.
33 F.-M. Xie, J.-X. Zhou, Y.-Q. Li and J.-X. Tang, *J. Mater. Chem. C*, 2020, **8**, 9476–9494.
34 C. H. Chen, J. Shi and C. W. Tang, *Macromol. Symp.*, 1998, **125**, 1–48.
35 M. Xie, M. Sun, S. Xue and W. Yang, *Dyes Pigm.*, 2023, **208**, 110799.
36 H. Nakanotani, T. Higuchi, T. Furukawa, K. Masui, K. Morimoto, M. Numata, H. Tanaka, Y. Sagara, T. Yasuda and C. Adachi, *Nat. Commun.*, 2014, **5**, 4016.
37 Y. Giret, J. Eng, T. Pope and T. Penfold, *J. Mater. Chem. C*, 2021, **9**, 1362–1369.
38 J. Adachi, H. Kakizoe, P. K. D. Tsang and A. Endo, *SID Int. Symp. Dig. Tech. Pap.*, 2019, **50**, 95–98.
39 D. Zhang, L. Duan, C. Li, Y. Li, H. Li, D. Zhang and Y. Qiu, *Adv. Mater.*, 2014, **26**, 5050–5055.
40 N. Haase, A. Danos, C. Pflumm, P. Stachelek, W. Brütting and A. P. Monkman, *Mater. Horiz.*, 2021, **8**, 1805–1815.
41 X. Wu, X. Peng, L. Chen, B. Z. Tang and Z. Zhao, *ACS Mater. Lett.*, 2023, **5**, 664–672.
42 Z. Chen, Q. Gu, M. Li, W. Qiu, Y. Jiao, X. Peng, W. Xie, D. Liu, K. Liu, Z. Yang and S.-J. Su, *Adv. Opt. Mater.*, 2024, **12**, 2302503.
43 J. Lv, Y. Huo, S. Xiao, Z. Zhao, L. Peng, Y. Liu, Z. Ren, D. Ma, S. Ying and S. Yan, *Mater. Chem. Front.*, 2023, **7**, 85–95.
44 J. Jayabharathi, S. Thilagavathy, V. Thanikachalam and J. Anudeebhana, *J. Mater. Chem. C*, 2022, **10**, 4342–4354.
45 A. Endo and P. K. D. Tang, *Dig. Tech. Pap. – Soc. Inf. Disp. Int. Symp.*, 2019, **50**, 360–362.
46 T. Baumann, M. Budzynski and C. Kasparek, *Dig. Tech. Pap. – Soc. Inf. Disp. Int. Symp.*, 2019, **50**, 466–469.
47 S. Y. Byeon, D. R. Lee, K. S. Yook and J. Y. Lee, *Adv. Mater.*, 2019, **31**, 1–15.
48 T. Förster, *Discuss. Faraday Soc.*, 1959, **27**, 7–17.
49 H. Wang, B. Yue, Z. Xie, B. Gao, Y. Xu, L. Liu, H. Sun and Y. Ma, *Phys. Chem. Chem. Phys.*, 2013, **15**, 3527.
50 N. Aizawa, S. Shikita and T. Yasuda, *Chem. Mater.*, 2017, **29**, 7014–7022.
51 K. Gao, K. Liu, X. L. Li, X. Cai, D. Chen, Z. Xu, Z. He, B. Li, Z. Qiao, D. Chen, Y. Cao and S. J. Su, *J. Mater. Chem. C*, 2017, **5**, 10406–10416.
52 W. Song, I. Lee and J. Y. Lee, *Adv. Mater.*, 2015, **27**, 4358–4363.
53 Y. J. Kang, J. H. Yun and J. Y. Lee, *Org. Electron.*, 2020, **78**, 105604.
54 Y. Wada, H. Nakagawa, S. Matsumoto, Y. Wakisaka and H. Kaji, *Nat. Photonics*, 2020, **14**, 643–649.
55 L.-S. Cui, A. J. Gillett, S.-F. Zhang, H. Ye, Y. Liu, X.-K. Chen, Z.-S. Lin, E. W. Evans, W. K. Myers, T. K. Ronson, H. Nakanotani, S. Reineke, J.-L. Bredas, C. Adachi and R. H. Friend, *Nat. Photonics*, 2020, **14**, 636–642.
56 D. H. Ahn, J. H. Jeong, J. Song, J. Y. Lee and J. H. Kwon, *ACS Appl. Mater. Interfaces*, 2018, **10**, 10246–10253.
57 Y. Wu, X. Liu, J. Liu, G. Yang, Y. Deng, Z. Bin and J. You, *J. Am. Chem. Soc.*, 2024, **146**, 15977–15985.
58 F. Wang, L. Zhang, W. Han, Z. Bin and J. You, *Angew. Chem., Int. Ed.*, 2022, **61**, e202205380.
59 J. H. Yun, K. H. Lee and J. Y. Lee, *Dyes Pigm.*, 2020, **181**, 108549.
60 J. S. Jang, S. H. Han, H. W. Choi, K. S. Yook and J. Y. Lee, *Org. Electron.*, 2018, **59**, 236–242.
61 J. S. Jang, S. H. Han and J. Lee, *Adv. Photonics Res.*, 2021, **2**, 2000109.
62 B. Sk, V. Thangaraji, N. Yadav, G. P. Nanda, S. Das, P. Gandeepan, E. Zysman-Colman and P. Rajamalli, *J. Mater. Chem. C*, 2021, **9**, 15583–15590.
63 M. Li, J. Wang, Y. Dai, Y. Zhang, L. Chen, L. Jin, Y. Tao, R. Chen and W. Huang, *J. Phys. Chem. C*, 2020, **124**, 1836–1843.
64 D. Zhang, X. Song, M. Cai and L. Duan, *Adv. Mater.*, 2018, **30**, 1705250.
65 U. Deori, N. Yadav, G. P. Nanda, K. L. Kumawat and P. Rajamalli, *ACS Appl. Electron. Mater.*, 2023, **5**, 4959–4967.
66 X. Song, D. Zhang, Y. Zhang, Y. Lu and L. Duan, *Adv. Opt. Mater.*, 2020, **8**, 1–10.
67 T. Nakamura, H. Sasabe, S. Abe, K. Kumada, R. Sugiyama, T. Hanayama and J. Kido, *Mol. Syst. Des. Eng.*, 2023, **8**, 866–873.
68 Z. Li, X. Hu, G. Liu, L. Tian, H. Gao, X. Dong, T. Gao, M. Cao, C. S. Lee, P. Wang and Y. Wang, *J. Phys. Chem. C*, 2021, **125**, 1980–1989.
69 Z. Li, X. Dong, G. Liu, L. Tian, X. Hu, T. Gao, H. Gao, Y. Qin, X. Gu, C. S. Lee, P. Wang, Y. Wang and Y. Liu, *Energy Fuels*, 2021, **35**, 19104–19111.
70 Y. H. Jung, D. Karthik, H. Lee, J. H. Maeng, K. J. Yang, S. Hwang and J. H. Kwon, *ACS Appl. Mater. Interfaces*, 2021, **13**, 17882–17891.

71 D. J. Shin, S. J. Hwang, J. Lim, C. Y. Jeon, J. Y. Lee and J. H. Kwon, *Chem. Eng. J.*, 2022, **446**, 137181.
72 W. Xie, X. Peng, M. Li, W. Qiu, W. Li, Q. Gu, Y. Jiao, Z. Chen, Y. Gan, K. kun Liu and S. J. Su, *Adv. Opt. Mater.*, 2022, **10**, 1–8.
73 J. Lee, U. Jo and J. Y. Lee, *ACS Appl. Mater. Interfaces*, 2023, **15**, 21261–21269.
74 T. Furukawa, H. Nakanotani, M. Inoue and C. Adachi, *Sci. Rep.*, 2015, **5**, 8429.
75 J. H. Kim, K. H. Lee and J. Y. Lee, *J. Mater. Chem. C*, 2020, **8**, 5265–5272.
76 S. K. Jeon, H. J. Park and J. Y. Lee, *ACS Appl. Mater. Interfaces*, 2018, **10**, 5700–5705.
77 D. Chen, X. Cai, X. Li, Z. He and C. Cai, *J. Mater. Chem. C*, 2017, **5**, 5223–5231.
78 G. Zhao, R. Zhou, G. Zhang, H. Chen, D. Ma, W. Tian, W. Jiang and Y. Sun, *J. Mater. Chem. C*, 2022, **10**, 5230–5239.
79 N. R. Wallwork, M. Mamada, A. Shukla, S. K. M. McGregor, C. Adachi, E. B. Namdas and S. C. Lo, *J. Mater. Chem. C*, 2021, **10**, 4767–4774.
80 Q. Zhang, B. Li, S. Huang, H. Nomura, H. Tanaka and C. Adachi, *Nat. Photonics*, 2014, **8**, 326–332.
81 J.-A. Seo, Y. Im, S. H. Han, C. W. Lee and J. Y. Lee, *ACS Appl. Mater. Interfaces*, 2017, **9**, 37864–37872.
82 D. Barman, K. Narang, R. Gogoi, D. Barman and P. K. Iyer, *J. Mater. Chem. C*, 2022, **10**, 8536–8583.
83 S. M. Leung, T. Chiu, C. Lin, J. Lee and M. Leung, *J. Mater. Chem. C*, 2019, **7**, 5874–5888.
84 I. H. Lee, W. Song, J. Y. Lee and S. H. Hwang, *J. Mater. Chem. C*, 2015, **3**, 8834–8838.
85 N. Boens, V. Leen and W. Dehaen, *Chem. Soc. Rev.*, 2012, **41**, 1130–1172.
86 J. Bañuelos, V. Martín, C. F. A. Gómez-Durán, I. J. A. Córdoba, E. Peña-Cabrera, I. García-Moreno, Á. Costela, M. E. Pérez-Ojeda, T. Arbeloa and Í. L. Arbeloa, *Chem.–Eur. J.*, 2011, **17**, 7261–7270.
87 A. Loudet and K. Burgess, *Chem. Rev.*, 2007, **107**, 4891–4932.
88 M. Chapran, E. Angioni, N. J. Findlay, B. Breig, V. Cherpak, P. Stakhira, T. Tuttle, D. Volyniuk, J. V. Grazulevicius, Y. A. Nastishin, O. D. Lavrentovich and P. J. Skabara, *ACS Appl. Mater. Interfaces*, 2017, **9**, 4750–4757.
89 J. V. Caspar, B. P. Sullivan, E. M. Kober and T. J. Meyer, *Chem. Phys. Lett.*, 1982, **91**, 91–95.
90 W. Zeng, T. Zhou, W. Ning, C. Zhong, J. He, S. Gong, G. Xie and C. Yang, *Adv. Mater.*, 2019, **31**, 1901404.
91 V. H. K. Fell, N. J. Findlay, B. Breig, C. Forbes, A. R. Inigo, J. Cameron, A. L. Kanibolotsky and P. J. Skabara, *J. Mater. Chem. C*, 2019, **7**, 3934–3944.
92 Q. Zhang, H. Kuwabara, W. J. Potscavage, S. Huang, Y. Hatae, T. Shibata and C. Adachi, *J. Am. Chem. Soc.*, 2014, **136**, 18070–18081.
93 W. Zeng, H.-Y. Lai, W.-K. Lee, M. Jiao, Y.-J. Shiu, C. Zhong, S. Gong, T. Zhou, G. Xie, M. Sarma, K.-T. Wong, C.-C. Wu and C. Yang, *Adv. Mater.*, 2018, **30**, 1704961.
94 S. Das, S. Kundu, B. Sk, M. Sarkar and A. Patra, *Org. Mater.*, 2021, **3**, 477–487.
95 A. Shukla, N. R. Wallwork, X. Li, J. Sobus, V. T. N. Mai, S. K. M. McGregor, K. Chen, R. J. Lepage, E. H. Krenske, E. G. Moore, E. B. Namdas and S. Lo, *Adv. Opt. Mater.*, 2020, **8**, 1901350.
96 X.-L. Li, G. Xie, M. Liu, D. Chen, X. Cai, J. Peng, Y. Cao and S.-J. Su, *Adv. Mater.*, 2016, **28**, 4614–4619.
97 S. Kundu, B. Sk, P. Pallavi, A. Giri and A. Patra, *Chem.–Eur. J.*, 2020, **26**, 5557–5582.
98 D. Das, P. Gopikrishna, D. Barman, R. B. Yathirajula and P. K. Iyer, *Nano Convergence*, 2019, **6**, 1–28.
99 G. He, L. Zheng and H. Yan, in *Proc. SPIE*, 2010, vol. 7852, p. 78520A.
100 K. T. Kamtekar, A. P. Monkman and M. R. Bryce, *Adv. Mater.*, 2010, **22**, 572–582.
101 T. Zhang, S.-J. He, D.-K. Wang, N. Jiang and Z.-H. Lu, *Sci. Rep.*, 2016, **6**, 20517.
102 N. Sun, Y. Zhao, F. Zhao, Y. Chen, D. Yang, J. Chen and D. Ma, *Appl. Phys. Lett.*, 2014, **105**, 13303.
103 J.-H. Jou, S.-M. Shen, C.-R. Lin, Y.-S. Wang, Y.-C. Chou, S.-Z. Chen and Y.-C. Jou, *Org. Electron.*, 2011, **12**, 865–868.
104 G. Zhou, Q. Wang, C.-L. Ho, W.-Y. Wong, D. Ma and L. Wang, *Chem. Commun.*, 2009, 3574–3576.
105 B. Zhao, T. Zhang, W. Li, Z. Su, B. Chu, X. Yan, F. Jin, Y. Gao and H. Wu, *Org. Electron.*, 2015, **23**, 208–212.
106 W. Song, I. H. Lee, S. H. Hwang and J. Y. Lee, *Org. Electron.*, 2015, **23**, 138–143.
107 D. Zhang, M. Cai, Y. Zhang, D. Zhang and L. Duan, *ACS Appl. Mater. Interfaces*, 2015, **7**, 28693–28700.
108 Z. Wu, L. Yu, X. Zhou, Q. Guo, J. Luo, X. Qiao, D. Yang, J. Chen, C. Yang and D. Ma, *Adv. Opt. Mater.*, 2016, **4**, 1067–1074.
109 F. M. Xie, S. J. Zou, Y. Li, L. Y. Lu, R. Yang, X. Y. Zeng, G. H. Zhang, J. Chen and J. X. Tang, *ACS Appl. Mater. Interfaces*, 2020, **12**, 16736–16742.
110 T. Higuchi, H. Nakanotani and C. Adachi, *Adv. Mater.*, 2015, **27**, 2019–2023.
111 H. Liu, J. Chen, Y. Fu, Z. Zhao and B. Z. Tang, *Adv. Funct. Mater.*, 2021, **31**, 2103273.
112 H. Liu, Y. Fu, B. Z. Tang and Z. Zhao, *Adv. Funct. Mater.*, 2023, **33**, 2309770.
113 Z. Liu, B. Zhao, Y. Gao, H. Chen, B. Dong, Y. Xu, J. Li, H. Wang and W. Li, *Opt. Mater.*, 2020, **110**, 110510.
114 S.-J. Zou, F.-M. Xie, Y.-Q. Li, Y.-Z. Shi, Y. Shen, Z.-G. Ma, J.-D. Chen, H.-X. Wei, X.-H. Zhang and J.-X. Tang, *Mater. Today Energy*, 2021, **21**, 100745.
115 Z. Wu, Q. Wang, L. Yu, J. Chen, X. Qiao, T. Ahamad, S. M. Alshehri, C. Yang and D. Ma, *ACS Appl. Mater. Interfaces*, 2016, **8**, 28780–28788.
116 X. Tang, Y. Li, Y. K. Qu, C. C. Peng, A. Khan, Z. Q. Jiang and L. S. Liao, *Adv. Funct. Mater.*, 2020, **30**, 1–8.
117 Y. Chen, Q. Sun, Y. Dai, D. Yang, X. Qiao and D. Ma, *J. Mater. Chem. C*, 2020, **8**, 13777–13785.
118 Z. Wang, X. L. Li, Z. Ma, X. Cai, C. Cai and S. J. Su, *Adv. Funct. Mater.*, 2018, **28**, 1–9.
119 H. Liu, Y. Fu, B. Z. Tang and Z. Zhao, *Nat. Commun.*, 2022, **13**, 5154.

120 P. Wei, D. Zhang and L. Duan, *Adv. Funct. Mater.*, 2020, **30**, 1907083.
121 S. Gottardi, M. Barbry, R. Coehoorn and H. van Eersel, *Appl. Phys. Lett.*, 2019, **114**, 73301.
122 H. Abroshan, V. Coropceanu and J.-L. Brédas, *ACS Mater. Lett.*, 2020, **2**, 1412–1418.
123 D. J. Shin, S. C. Kim and J. Y. Lee, *J. Mater. Chem. C*, 2022, **10**, 4821–4830.
124 D. L. Dexter, *J. Chem. Phys.*, 2004, **21**, 836–850.
125 Y. Zhang and S. R. Forrest, *Chem. Phys. Lett.*, 2013, **590**, 106–110.
126 S. H. Han and J. Y. Lee, *J. Mater. Chem. C*, 2018, **6**, 1504–1508.
127 W. J. Chung and J. Y. Lee, *J. Inf. Disp.*, 2021, **22**, 49–54.
128 M. I. Alam, M. R. Nagar, S. R. Nayak, A. Choudhury, J. Jou and S. Vaidyanathan, *Adv. Opt. Mater.*, 2022, **10**, 2200376.
129 K. Bartkowski, P. Zimmermann Crocomo, M. A. Kochman, D. Kumar, A. Kubas, P. Data and M. Lindner, *Chem. Sci.*, 2022, **13**, 10119–10128.
130 B. Zhao, Z. Su, W. Li, B. Chu, F. Jin, X. Yan, T. Zhang, F. Zhang, D. Fan, Y. Gao, J. Wang, H. Pi and J. Zhu, *Nanoscale Res. Lett.*, 2013, **8**, 529.
131 S. H. Kim, J. Jang, J.-M. Hong and J. Y. Lee, *Appl. Phys. Lett.*, 2007, **90**, 173501.
132 M. Jakoby, B. S. Richards, U. Lemmer and I. A. Howard, *Phys. Rev. B*, 2019, **100**, 45303.
133 H. Hirai, K. Nakajima, S. Nakatsuka, K. Shiren, J. Ni, S. Nomura, T. Ikuta and T. Hatakeyama, *Angew. Chem.*, 2015, **127**, 13785–13789.
134 T. Hatakeyama, K. Shiren, K. Nakajima, S. Nomura, S. Nakatsuka, K. Kinoshita, J. Ni, Y. Ono and T. Ikuta, *Adv. Mater.*, 2016, **28**, 2777–2781.
135 G. Liu, H. Sasabe, K. Kumada, A. Matsunaga, H. Katagiri and J. Kido, *J. Mater. Chem. C*, 2021, **9**, 8308–8313.
136 X. Liang, Z. Yan, H. Han, Z. Wu, Y. Zheng, H. Meng, J. Zuo and W. Huang, *Angew. Chem., Int. Ed.*, 2018, **57**, 11316–11320.
137 Y. J. Yu, F. M. Liu, X. Y. Meng, L. Y. Ding, L. S. Liao and Z. Q. Jiang, *Chem.–Eur. J.*, 2023, **29**, e202202628.
138 S. Ji, G. Xie and Q. Xue, *Flexible Printed Electron.*, 2023, **8**, 033003.
139 X. Cai, J. Xue, C. Li, B. Liang, A. Ying, Y. Tan, S. Gong and Y. Wang, *Angew. Chem., Int. Ed.*, 2022, **61**, e202200337.
140 S. Wu, A. Kumar Gupta, K. Yoshida, J. Gong, D. Hall, D. B. Cordes, A. M. Z. Slawin, I. D. W. Samuel and E. Zysman-Colman, *Angew. Chem., Int. Ed.*, 2022, **61**, e202213697.
141 K. Zhang, X. Wang, Y. Chang, Y. Wu, S. Wang and L. Wang, *Angew. Chem., Int. Ed.*, 2023, **62**, e202313084.
142 D. Hall, S. M. Suresh, P. L. dos Santos, E. Duda, S. Bagnich, A. Pershin, P. Rajamalli, D. B. Cordes, A. M. Z. Slawin, D. Beljonne, A. Köhler, I. D. W. Samuel, Y. Olivier and E. Zysman-Colman, *Adv. Opt. Mater.*, 2020, **8**, 1901627.
143 Y. Kondo, K. Yoshiura, S. Kitera, H. Nishi, S. Oda, H. Gotoh, Y. Sasada, M. Yanai and T. Hatakeyama, *Nat. Photonics*, 2019, **13**, 678–682.
144 C. Y. Chan, M. Tanaka, Y. T. Lee, Y. W. Wong, H. Nakanotani, T. Hatakeyama and C. Adachi, *Nat. Photonics*, 2021, **15**, 203–207.
145 M. Mamada, H. Katagiri, C. Y. Chan, Y. T. Lee, K. Goushi, H. Nakanotani, T. Hatakeyama and C. Adachi, *Adv. Funct. Mater.*, 2022, **32**, 2204352.
146 H. Lee, R. Braveenth, S. Muruganantham, C. Y. Jeon, H. S. Lee and J. H. Kwon, *Nat. Commun.*, 2023, **14**, 419.
147 S. H. Han, J. H. Jeong, J. W. Yoo and J. Y. Lee, *J. Mater. Chem. C*, 2019, **7**, 3082–3089.
148 H. Mubarok, A. Amin, T. Lee, J. Jung, J.-H. Lee and M. H. Lee, *Angew. Chem., Int. Ed.*, 2023, **62**, e202306879.
149 K. Stavrou, S. Madayanad Suresh, D. Hall, A. Danos, N. A. Kukhta, A. M. Z. Slawin, S. Warriner, D. Beljonne, Y. Olivier, A. Monkman and E. Zysman-Colman, *Adv. Opt. Mater.*, 2022, **10**, 1–21.
150 Y. Hu, J. Miao, C. Zhong, Y. Zeng, S. Gong, X. Cao, X. Zhou, Y. Gu and C. Yang, *Angew. Chem., Int. Ed.*, 2023, **62**, e202302478.
151 K. Stavrou, L. G. Franca, A. Danos and A. P. Monkman, *Nat. Photonics*, 2024, **18**, 554–561.
152 S. O. Jeon, K. H. Lee, J. S. Kim, S. G. Ihn, Y. S. Chung, J. W. Kim, H. Lee, S. Kim, H. Choi and J. Y. Lee, *Nat. Photonics*, 2021, **15**, 208–215.
153 K. H. Lee and J. Y. Lee, *Adv. Opt. Mater.*, 2020, **8**, 2000328.
154 K. Kishore Kesavan, J. Jayakumar, M. Lee, C. Hexin, S. Sudheendran Swayamprabha, D. Kumar Dubey, F.-C. Tung, C.-W. Wang and J.-H. Jou, *Chem. Eng. J.*, 2022, **435**, 134879.
155 K. Goushi and C. Adachi, *Appl. Phys. Lett.*, 2012, **101**, 23306.
156 K. Goushi, K. Yoshida, K. Sato and C. Adachi, *Nat. Photonics*, 2012, **6**, 253–258.
157 Q. Wang, Q. Tian and Y. Zhang, *J. Mater. Chem. C*, 2019, **7**, 11329–11360.
158 M. Sarma and K.-T. Wong, *ACS Appl. Mater. Interfaces*, 2018, **10**, 19279–19304.
159 X.-K. Liu, Z. Chen, C.-J. Zheng, M. Chen, W. Liu, X.-H. Zhang and C.-S. Lee, *Adv. Mater.*, 2015, **27**, 2025–2030.
160 K.-H. Kim, C.-K. Moon, J. W. Sun, B. Sim and J.-J. Kim, *Adv. Opt. Mater.*, 2015, **3**, 895–899.
161 B. Zhao, T. Zhang, B. Chu, W. Li, Z. Su, H. Wu, X. Yan, F. Jin, Y. Gao and C. Liu, *Sci. Rep.*, 2015, **5**, 10697.
162 W.-Y. Hung, P.-Y. Chiang, S.-W. Lin, W.-C. Tang, Y.-T. Chen, S.-H. Liu, P.-T. Chou, Y.-T. Hung and K.-T. Wong, *ACS Appl. Mater. Interfaces*, 2016, **8**, 4811–4818.
163 T. B. Nguyen, H. Nakanotani, T. Hatakeyama and C. Adachi, *Adv. Mater.*, 2020, **32**, 1906614.
164 B. Liang, J. Wang, Z. Cheng, J. Wei and Y. Wang, *J. Phys. Chem. Lett.*, 2019, **10**, 2811–2816.
165 D. Li, Y. Hu and L. S. Liao, *J. Mater. Chem. C*, 2019, **7**, 977–985.
166 Q. Wang, L. Chen, Q. Yang, Y. Xu, H. Wang and Z. Xie, *Adv. Mater. Interfaces*, 2022, **9**, 2200830.
167 S.-W. Wen, M.-T. Lee and C. H. Chen, *J. Disp. Technol.*, 2005, **1**, 90–99.
168 D. Y. Kondakov, *Philos. Trans. R. Soc., A*, 2015, **373**, 20140321.

169 F. Xie, X. Yang, P. Jin, X. Wang, H. Ran, H. Zhang, H. Sun, S. Su and J. Hu, *Adv. Opt. Mater.*, 2023, **11**, 2202490.
170 H. Nakanotani, K. Masui, J. Nishide, T. Shibata and C. Adachi, *Sci. Rep.*, 2013, **3**, 2127.
171 M. Kim, S. K. Jeon, S.-H. Hwang and J. Y. Lee, *Adv. Mater.*, 2015, **27**, 2515–2520.
172 S. K. Jeon, H. L. Lee, K. S. Yook and J. Y. Lee, *Adv. Mater.*, 2019, **31**, 1803524.
173 Q. Wang and H. Aziz, *ACS Appl. Mater. Interfaces*, 2013, **5**, 8733–8739.
174 K. Thakur, B. van der Zee, G.-J. A. H. Wetzelaer, C. Ramanan and P. W. M. Blom, *Adv. Opt. Mater.*, 2022, **10**, 2101784.
175 D. Karthik, D. H. Ahn, J. H. Maeng, H. Lee, H. Yoo, R. Lampande, J. Y. Lee and J. H. Kwon, *Dig. Tech. Pap. – Soc. Inf. Disp. Int. Symp.*, 2020, **51**, 61–64.
176 J. Y. Kim, T. R. Hong, I. R. Choe, J. A. Lee, H. G. Ryu, B. M. Seo, J. H. Yang, C. W. Han, J. H. Baek, H. C. Choi and I. B. Kang, *Dig. Tech. Pap. – Soc. Inf. Disp. Int. Symp.*, 2020, **51**, 53–56.
177 J.-M. Kim, C.-H. Lee and J.-J. Kim, *Appl. Phys. Lett.*, 2017, **111**, 203301.
178 A. Pinato, A. Cester, M. Meneghini, N. Wrachien, A. Tazzoli, S. Xia, V. Adamovich, M. S. Weaver, J. J. Brown, E. Zanoni and G. Meneghesso, *IEEE Trans. Electron Devices*, 2010, **57**, 178–187.
179 A. Endo, H. Kakizoe, T. Oyamada and J. Adachi, *Dig. Tech. Pap. – Soc. Inf. Disp. Int. Symp.*, 2020, **51**, 57–60.
180 J. Adachi, S. Otsu, H. Kakizoe and T. Oyamada, *SID Int. Symp. Dig. Tech. Pap.*, 2021, **52**, 232–235.